iScience

CellPress
OPEN ACCESS

Article

Making solar electricity dispatchable: A technical and economic assessment of the main conversion and storage technologies

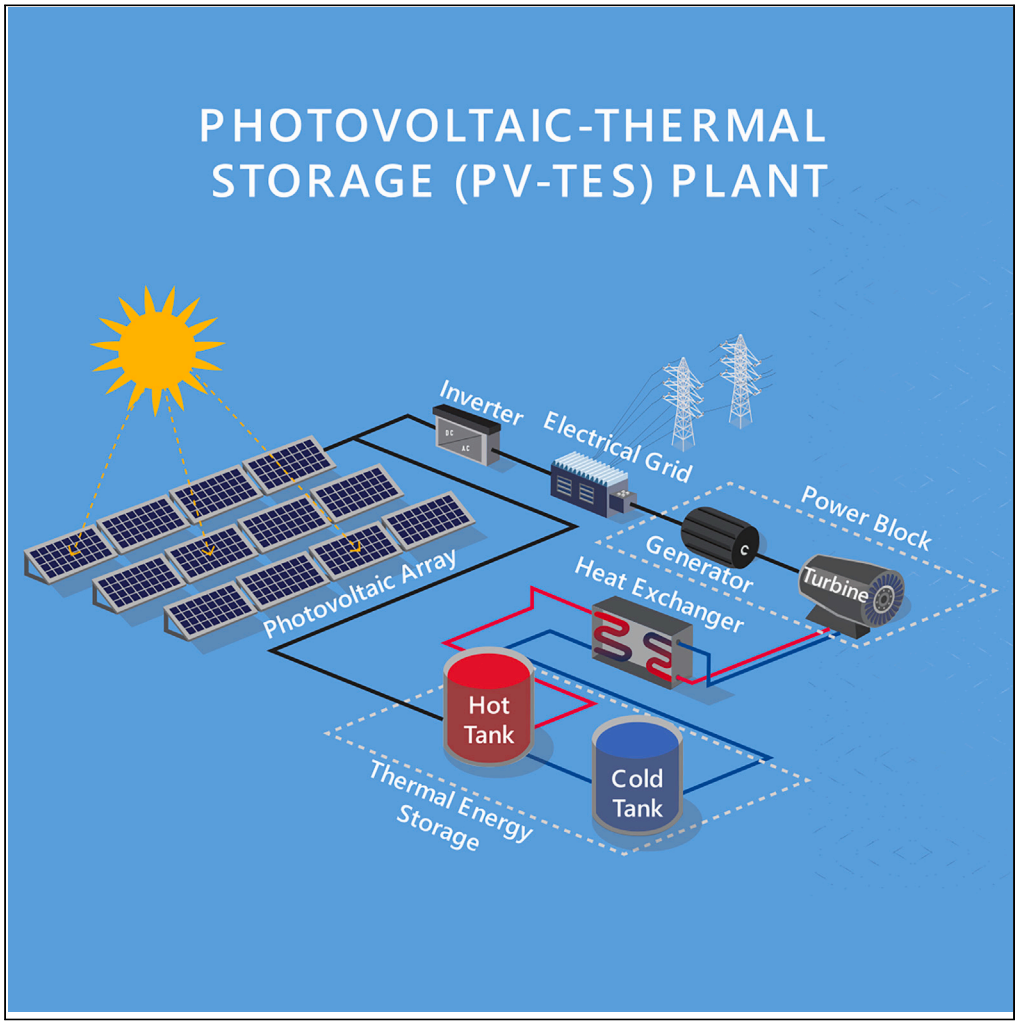

Freddy Ordóñez, Thomas Fasquelle, Alain Dollet, Alexis Vossier

alexis.vossier@promes.cnrs.fr

Highlights

The techno-economic performances of 5 different solar technologies was assessed

The increase in the dispatchability of the solar plants leads to additional energy losses

Technologies involving thermal storage offer the best techno-economic indicators

Ordóñez et al., iScience 26, 108028
November 17, 2023 © 2023 The Author(s).
https://doi.org/10.1016/j.isci.2023.108028

iScience

CellPress
OPEN ACCESS

Article

Making solar electricity dispatchable: A technical and economic assessment of the main conversion and storage technologies

Freddy Ordóñez,[1,4] Thomas Fasquelle,[2,4] Alain Dollet,[3] and Alexis Vossier[3,4,5,*]

SUMMARY

The techno-economic performances of five different solar-electricity conversion technologies (photovoltaic, solar tower, parabolic trough as well as two hybrid PV/CSP systems) associated with three energy storage means (electrochemical, thermal, and thermophotovoltaic) are evaluated thanks to representative models applied to four representative sites around the world. The evaluation is based on the ability to dispatch the power production throughout the year, the ability to maximize energy injection in the electrical grid, and the levelized cost of electricity. It is found that increasing the dispatchability of solar power plants will necessarily lead to the emergence of additional energy losses and important LCOE increase, either because of low round-trip efficiency of the storage system, or because of its high cost of energy capacity. Despite lower energy production for a given collecting area, combination of PV power plants with electrochemical storage or thermal energy storage surprisingly seem to be the most promising paths.

INTRODUCTION

The deployment of solar power has known a tremendous growth in the last decades. PV is by far the most deployed technology worldwide, owing to its low prices: PV prices below 11 USD/MWh[1] have been reported in the sunniest areas, and PV power is already among the cheapest electricity sources in many countries.[2] The installed capacity of PV modules has exceeded the TW level in 2022,[3] and the share of solar electricity in the world electricity mix is now close to 5%.[4]

Despite these encouraging trends, the growth of solar power beyond its current level is hindered by the low dispatchability of these technologies. Because of its intermittent nature, the injection of solar power in the electrical grid is fundamentally constrained by the availability of the solar resource, leading to discrepancies between electricity production and demand. For low penetration levels of solar power in the grid, the variability of the solar input can be balanced by adjusting the electrical production from other dispatchable means (i.e., natural gas, hydro, or nuclear plants). However, correcting this mismatch becomes more intricate as the share of variable renewable energy (VRE) plants increases, leading to growing electricity curtailments,[5] as well as increased occurrences of negative electricity prices in the energy markets.[6]

Further deployment of VRE in the electricity mix will thus require the development of storage solutions aiming at smoothing solar electricity production and therefore achieving a better matching with the electrical demand. Number of storage technologies are currently under development, covering a wide range of time response, power, and energy characteristics, such as battery energy storage systems (BESS),[7] pumped hydro energy storage (PHS),[8] flywheels,[9] compressed-air energy systems (CAES),[10] or thermal energy storage (TES) systems.[11] Because of their cost structure, their efficiency, or their typical operating conditions, the techno-economic performances of each storage technology may vary significantly depending on the storage characteristics (i.e., capacity, power), the dispatch strategy of the electrical energy stored (i.e., baseload or tracking load), or the targeted dispatchability of the plant. The ability of solar and wind energy to cover an increasing fraction of the electric demand has been already evaluated both at the level of the US,[12] and at the world level.[13]

A number of works published over the last years aimed at finding the optimal designs of solar plants to maximize electricity production and/or to minimize electricity costs while achieving a given dispatchability for selected geographical locations, most often comparing the performances of the different solutions proposed. The operation of specific solar plant technology designed to achieve a given dispatchability was recently discussed for concentrated solar power (CSP) including TES,[14] with the possible addition of a PV field (with or without electrochemical storage) leading in some cases to non-compact hybrid PV-CSP plants whose performances are finally compared to stand-alone configurations.[15–18] Most often, this kind of integrated non-compact PV-CSP plants has turned out to decrease electricity costs as compared to

[1]Departamento de Ingeniería Mecánica, Escuela Politécnica Nacional, Ladrón de Guevara E11-275, Quito, Ecuador
[2]Aix Marseille Université, CNRS, IUSTI, Marseille, France
[3]CNRS, Laboratoire PROcédés, Matériaux et Energie Solaire (PROMES), UPR 8521, 7 Rue Du Four Solaire, 66120 Odeillo, France
[4]These authors contributed equally
[5]Lead contact
*Correspondence: alexis.vossier@promes.cnrs.fr
https://doi.org/10.1016/j.isci.2023.108028

This is an open access article under the CC BY-NC-ND license (http://creativecommons.org/licenses/by-nc-nd/4.0/).

stand-alone plants or non-integrated hybrid plants (where the PV and CSP parts operate independently).[18–21] These recent studies offer useful insights regarding the ability of solar power to guarantee dispatchable electricity production at minimum cost, provided that the storage volume and the solar plant peak power are finely tailored. However, it is usually difficult to draw generic conclusions from these previous works since they are often specific to 1 or 2 geographical locations[15,16,18,21–24] and/or to a restricted number of technological options or consider a rudimentary demand scenario (such as baseload).[15,23] It is difficult, for instance, to conclude on the interest of having both BESS and TES to store the excess electricity. Some very recent works have considered a rather wide set of solar plant configurations combining CSP, PV, TES, and BESS and determined the technological combinations leading to the lowest electricity cost allowing to satisfy a given demand fraction[18] or to minimize the loss of power supply probability (LPSP)[21,25]: they have shown that TES is required to minimize the levelized cost of electricity (LCOE) and better meet the demand but they have drawn different conclusions on the interest of adding BESS; however, each study considered a single but different geographical location. Other recent studies have considered rather larger sets of different geographical sites and technological configurations but simplified demand scenarios, e.g., prioritize production at night.[26,27] Although most articles considering economic criteria for solar plant optimization focused only or mostly on the LCOE, some recent papers have also included the energy markets in their multi-objective optimization, e.g., in[28] to maximize the benefit-to-cost ratio according to the fluctuating market prices. Sensitivity analyses on the cost of key plant components such as storage systems or projection of costs have sometimes been included in the optimization.[16,17,21,26,29] Another group of studies has more specifically focused on the value of different storage technologies, such as PHS, CAES, and BESS, for a given VRE mix in a given location. These studies concluded that the integration of additional generation capacity combined with energy curtailment may outperform strategies involving additional storage integration.[30–32] The latter is however more effective in decarbonizing the energy produced,[33] and a combination of long-term and short-term energy storage may constitute an optimal solution.[34] It has also been shown that energy capacity cost and discharge efficiency are the most important parameters in terms of revenue optimization for a given demand, compared to load efficiency and capacity cost. Thus, the low round-trip efficiency of several storage technologies (such as hydrogen) may put a damper on their competitiveness.[35]

Here, we extend these previous analyses by providing a benchmark study aiming at evaluating how the different conversion and storage technologies behave and compare to each other on some technical and economic grounds. In particular, we aim at (1) identifying and comparing the main energy loss sources involved depending on the targeted dispatchability, (2) evaluating how the increased dispatchability may affect some key economic indicators of the plants, (3) discussing some key component to be improved toward lowering the cost of dispatchable solar electricity. Our analysis includes widely deployed solar and storage technologies (such as PV and electrochemical storage, and to a lesser extent, CSP) but also emerging technologies that have raised interest recently owing to their supposedly improved technical or economic performances (such as hybrid PV-CSP solar plants, TES or thermophotovoltaic batteries (TPVB)). We use an in-house model to evaluate the annual electricity generation and the ability of the different plants investigated to satisfy a predefined electrical load. Then, we introduce indicators aimed at quantifying the amplitude of the main energy loss across a wide range of storage volumes and solar plant peak powers. Finally, we compute the levelized cost of electricity over a large range of dispatchabilities, and conclude with an evaluation of the economic benefits associated with a cost decrease of some key component of the plants under investigation. The seven conversion + storage technologies investigated in this work are depicted schematically in Figure 1.

RESULTS

Maximum electricity production

We first start by evaluating the maximum electrical energy delivered by each plant technology and for each site under investigation, assuming that the electrical energy produced is directly injected in the grid, without any losses. This first evaluation, shown in Figure 2 thus provides an upper limit of the maximum electrical energy generated by each individual plant under investigation, without any operational constraint on the dispatch strategy adopted.

Because the estimations are based upon the assumption of an identical collection area of each plant, the values reported here only allows an energy comparison per unit area of collector, and does not reflect the inherent superiority of one or another solar technology per unit of land. This first estimate is however required to derive the mean power generation one can expect from each solar technology in each site. In the following, this mean power generation value $\overline{P}$ (simply calculated as the annual energy output divided by the number of hours in a year) will serve as a reference power indicator, allowing fair comparisons between technologies and sites to be realized. Several preliminary conclusions can be drawn:

- hybrid PV/CSP systems systematically show higher annual energy yields over competing solar technologies. In particular, the PV mirror approach leads to higher energy yields in each site, as a result of its improved ability to better harness diffuse radiation.
- while CSP does not demonstrate any improvement over conventional PV plants in moderate insolation sites, we observe a significant gain in the energy output of CSP plants at highly insolated sites.

Table 1 summarizes the maximum annual electrical energy (E_{max}) delivered by each plant, assuming that the electricity is directly injected in the grid, without losses. $\overline{P}_{BL}$ denotes the electrical power which should be continuously injected in the grid (24h/day, 365 days per year) to deliver the same energy output, and will serve as a basis for the upcoming estimates.

From intermittent to dispatchable power generation

Shifting from intermittent to dispatchable solar electricity production induces additional constraints on the plant operation, which should satisfy a predefined electrical load rather than intermittently injecting solar electricity in the grid. Two distinct dispatch strategies may be

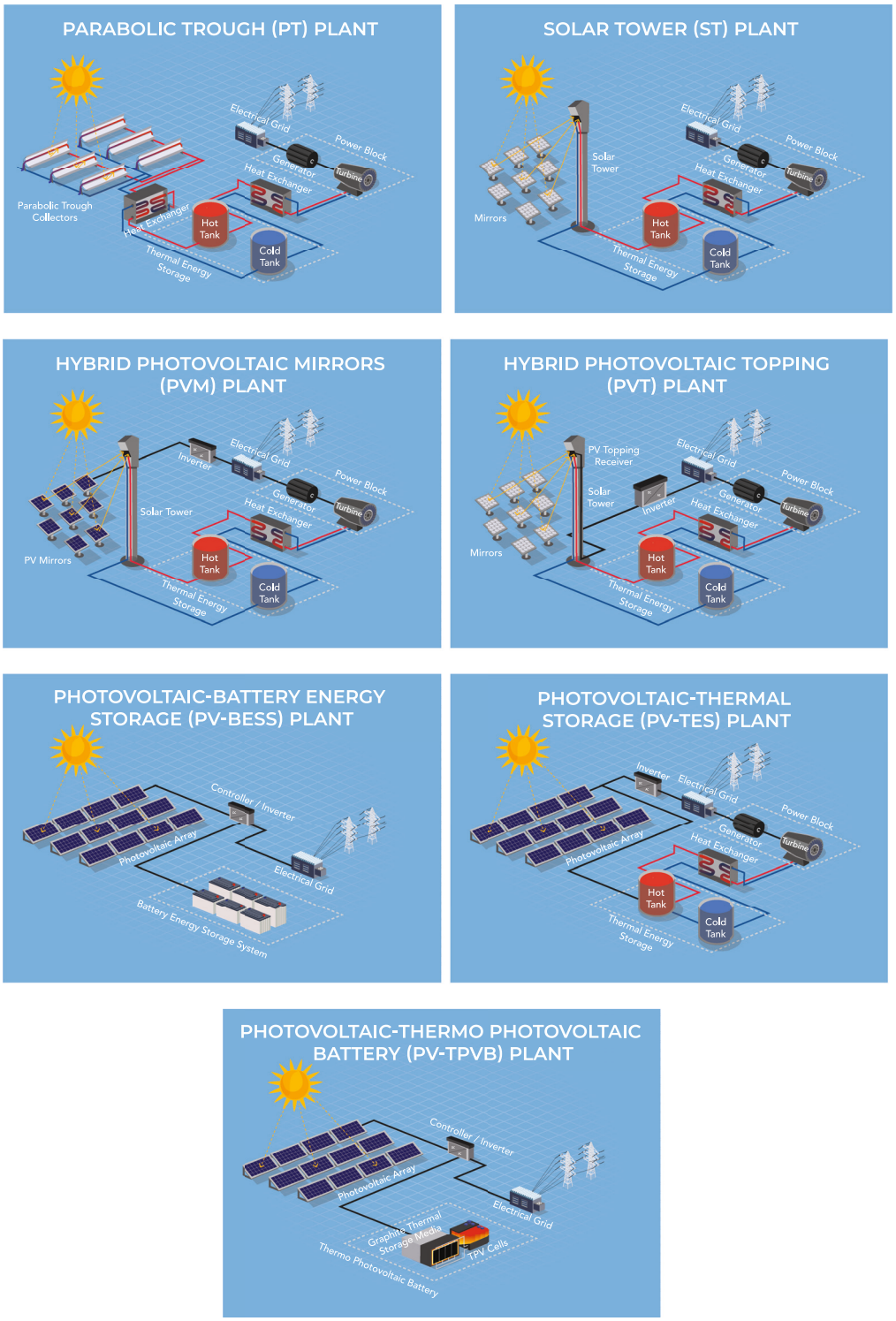

Figure 1. Schematic representation of the seven combinations of solar energy conversion and storage technologies studied

considered, namely 1) *baseload (BL)* electricity generation, where the electrical power injected in the grid is assumed to hold a constant value throughout the year 2) *tracking load (TL)* electricity generation, where the electrical power injected in the grid is assumed to follow the electrical demand profile of the region/country where the solar plant is operated.

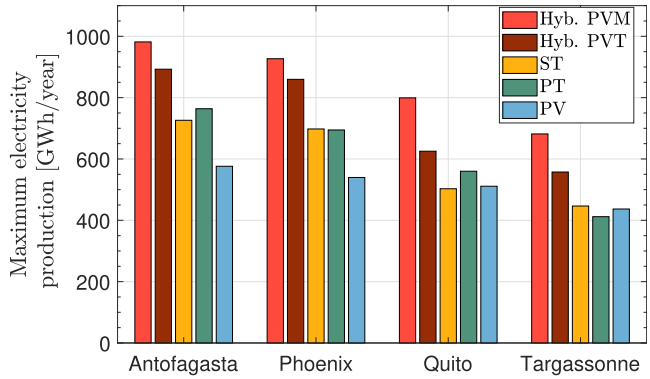

Figure 2. Maximum annual electricity production of the 5 solar technologies under investigation at Antofagasta (Chile), Phoenix (USA), Quito (Equator) and Targasonne (France)

The load applied to the different solar plants under investigation is logically tailored to the electrical energy these plants are likely to deliver in the absence of any operational constraints, following the steps described below.

- the instantaneous averaged electrical load is assumed to follow the electrical demand, and is calculated on an hourly basis as:

$$\overline{P}_L(t) = \frac{D(t)}{\sum_{i=1}^{8760} D(t) \cdot \Delta t_{step}} \times E_{max} \quad \text{(Equation 1)}$$

where $D(t)$ refers to the hourly energy demand of the country/region where the solar plant of interest is operated and Δt_{step} is the timestep of the simulation: 1 h. The summation of $\overline{P}_L$ over each hour of a year is thus equal to E_{max}.

- we explore the techno-economic performances of the different plants over a wide range of electrical loads by applying a *load factor f* to the reference electrical load $\overline{P}_L$. In doing so, the shape of the electrical load is kept identical, and the power demanded from the plant is either increased (load factor > 1) or decreased (load factor < 1) relative to the reference load value $\overline{P}_L$.

In the following, the electrical load imposed to the different plants investigated will simply be given by:

Table 1. Maximum electrical energy delivered by the five solar plant technologies investigated at Antofagasta (Chile), Phoenix (USA), Quito (Equator) and Targasonne (France)

	Hybrid PVM	Hybrid PVT	ST	PT	PV
Antofagasta (Chile)					
E_{max} [GWh_{el} /year]	981.7	892.8	726.2	763.9	576.2
Φ_{max} [GWh_{el} /(km^2.year)]	141	142	116	191	181
$\overline{P}_{BL}$ [MWh_{el} /h]	112.1	101.9	82.9	87.2	65.8
Phoenix (USA)					
E_{max} [GWh_{el} /year]	926.9	859.7	697.9	694.6	539.7
Φ_{max} [GWh_{el} /(km^2.year)]	134	137	112	174	169
$\overline{P}_{BL}$ [MWh_{el} /h]	105.8	98.1	79.7	79.3	61.6
Quito (Equator)					
E_{max} [GWh_{el} /year]	799.3	625.3	502.9	560.0	511.1
Φ_{max} [GWh_{el} /(km^2.year)]	113	99	80	140	160
$\overline{P}_{BL}$ [MWh_{el} /h]	91.2	71.4	57.4	63.9	58.3
Targassonne (France)					
E_{max} [GWh_{el} /year]	681.6	557.5	446.6	411.8	436.9
Φ_{max} [GWh_{el} /(km^2.year)]	98	89	72	103	137
$\overline{P}_{BL}$ [MWh_{el} /h]	77.8	63.6	51.0	47.0	49.9

$$P_L = f \times \overline{P}_L \quad \text{(Equation 2)}$$

where f is the load factor and $\overline{P}$ refers to the tracking load reference value.

Note that a load factor >1 cannot be satisfied on a yearly timescale, the electrical demand integrated over a year of operation exceeding the total maximal energy E_{max} likely to be delivered (Table 1). However, imposing high electrical loads will constrain the different solar plants to inject a larger fraction of their electricity production directly on the electrical grid. As a consequence, the lower energy surplus available for increasing load factors will necessarily reduce the energy available for storage. Conversely, imposing lower load factors will lessen the electrical power demanded from the plant, and favor storage of energy for delayed use.

Integration of storage: technical assessment

The joint quest for dispatchability and restitution is motivated by the need to simultaneously satisfy the electrical demand, imposed by the power grid, while maximizing the electrical power actually injected into the grid. The value placed on energy restitution or dispatchability logically depends on numerous technical and economic parameters, such as grid stability, the value of electricity on the energy market, the cost of the plant, or the costs associated with intermittent plant operation. Identifying the operating conditions that lead to optimum values of dispatchability and restitution is therefore a complex task, which is largely dependent on the plant's characteristics, the electrical demand profile and the economic framework governing its operation. The ability of storage to smooth solar electricity production and adapt it to a given electrical load profile is assessed here on the basis of complementary indicators.

Restitution efficiency

This indicator quantifies the ability of a given solar plant to efficiently inject on the grid the electrical energy produced over a year. The *restitution* efficiency corresponding to a given combination of electrical load power (P_L) and storage volume (S) is given by:

$$\eta_{rst}(P_L, S) = \frac{E(P_L, S)}{E_{max}} \quad \text{(Equation 3)}$$

where $E(P_L, S)$ is the effective annual energy production of a power plant operated to fulfill an electrical load P_L with a storage volume S (expressed in *MWh*). The maximum annual energy production E_{max} provides an upper bound to the energy likely to be injected in the electrical grid, and an efficient storage system should logically show a restitution efficiency as close to 1 as possible.

Dispatch efficiency

The restitution efficiency is not sufficient, by itself, to catch the ability of a given system to adapt the electricity production to the load profile requested. The *dispatch* efficiency is introduced here to quantify the ability of a given storage capacity S to satisfy an electrical load P_L imposed to the plant throughout the year. The dispatch efficiency can be written:

$$\eta_{dp}(P_L, S) = \frac{E(P_L, S)}{\sum_{i=1}^{8760} P_L(t) \cdot \Delta t_{step}} \quad \text{(Equation 4)}$$

where $P_L(t)$ refers to the electrical load imposed to the solar plant. High values of the dispatch efficiency are requested to guarantee a satisfaction of the load throughout the year.

Overall performance indicator

Satisfying simultaneously a high energy restitution on the electrical grid and a high dispatch efficiency may be an intricate problem. Since dispatch and restitution efficiencies are linked through the relation $\eta_{rst} = f \cdot \eta_{dp}$, maximizing one of these indicators will necessarily be detrimental to the other. To better identify the operating conditions (in terms of storage duration and electrical load) likely to lead to storage indicators consistent with the technical expectations of the plant operators, we introduce an *overall performance indicator* of the storage. This indicator encompasses both the restitution and the dispatch capabilities of a given combination of electrical load and storage volume, and is simply calculated as:

$$\eta_{rst}(P_L, S) \times \eta_{dp}(P_L, S) \quad \text{(Equation 5)}$$

Figure 3 shows the electrical energy effectively injected on the electrical grid (A), the restitution efficiency η_{rst} (B), the dispatch efficiency η_{dp} (C), as well as the overall performance indicator of the storage $\eta_{dp} \times \eta_{rst}$ (D) for the PV + BESS technology as a function of the load factor f applied to the plant, and for storage duration up to 24 h, in Targasonne, France (the curves corresponding to the other 3 sites and the 6 other technologies under investigation can be found in Figures S2–S28 in the supplemental information).

We notice large variations in the electrical energy effectively delivered to the grid depending on both the typical load factor applied to the plant and the storage duration. Achieving high energy output requires the plant to be operated at high load factor, with significant storage duration (the amount of storage required being logically function of the load factor applied to the plant). The analysis of the *restitution* efficiency, which logically scales with the energy effectively delivered to the grid, confirms that high restitution efficiency values can only be achieved for sufficiently high load factors. Conversely, the *dispatch* efficiency is maximized at low load factors, and large amounts of storage are also required toward attaining dispatch efficiencies approaching 1. The discrepancy between these two trends stresses a fundamental

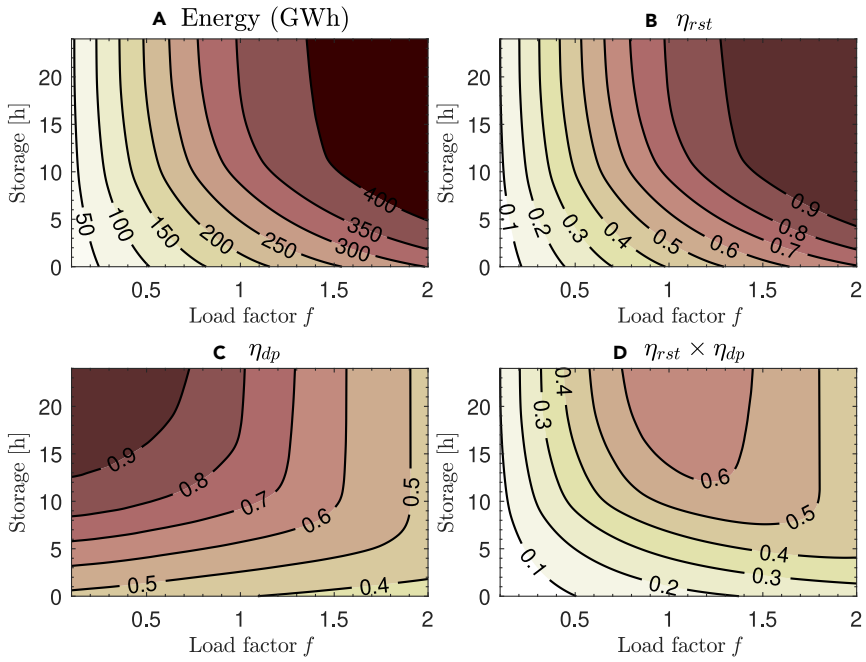

Figure 3. Overall performance indicators for the PV + BESS technology in Targasonne, France

limitation of solar technologies including storage: simultaneously attaining high dispatchability and high energy restitution on the electrical grid is a practically complex task. The overall performance indicator, shown in Figure 3D) reveals the existence of a trade-off between dispatchability and restitution which, in the specific case of PV + BESS, is attained at load factors slightly exceeding 1 and for storage durations exceeding 15 to 20 h (recall that dispatchability and restitution are equally weighted in our analysis). Figures 4 and 5 illustrate the variation of the different storage indicators (η_{dp}, η_{rst}, and $\eta_{dp} \times \eta_{rst}$) for the 7 solar + storage combinations considered here (namely: 1) Parabolic Trough 2) Solar Tower 3) PV-Mirror Hybrid PV-CSP 4) PV-Topping Hybrid PV-CSP 5) PV + TES 6) PV + BESS 7) PV + TPVB), in Targasonne (Figure 4) and Antofagasta (Figure 5). The 3 upper sub-figures show the different performance indicators as a function of the load factor considering a storage duration equivalent to 2 h at peak operation, while the 3 intermediate and the 3 lower sub-figures respectively illustrate the evolution of these performance indicators for storage duration of 8h and 24h.

The analysis of Figures 4 and 5 reveals the existence of 3 distinct regimes.

1. At sufficiently low load factors and sufficiently high storage duration, the solar plant is fully dispatchable and further increasing the storage duration, or lowering the load factor, does not provide any additional dispatchability gain. This translates into the existence of a threshold load factor value below which the plant dispatchability reaches a *plateau*, while the restitution efficiency decreases linearly, independently of the storage characteristics. Such a situation can clearly be identified at Antofagasta, for a storage duration of 24 h and for load factors < 0.5.
2. There is an extended range of load factor values over which the nature and the characteristics of the storage affect the *dispatchability-restitution* capabilities of the plants. The performance of a given storage technology is primarily dictated by its roundtrip efficiency, but also by the storage volume integrated in the plant. Overall, PV plants integrating either BESS, TES or TPVB surpass CSP plants in terms of storage performance for short storage duration at moderately insolated sites (such as Targasonne (Figure 4) and Quito (Figure S29)). For increasing storage volumes, CSP systems involving thermal energy storage progressively outperform PV plants integrating thermal energy storage (TES or TPVB) because of the fundamentally inefficient *electricity* → *heat* → *electricity* process of these latter. The magnitude of the gap separating CSP and hybrid PV/CSP on the one hand, and PV + TES or PV + TPVB on the other hand, is even more pronounced in the most insolated sites: these technologies offer *dispatchability-restitution* performance that are comparable to conventional PV plants integrating batteries.
3. For high load factors, the solar plants are requested to inject an increasing fraction of the energy generated directly on the grid, without being stored beforehand. As a consequence, the *dispatchability-restitution* indicators tend to get closer to each other.

Several additional observations can be made.

- For a storage duration of 2 h, we observe a weak dependence of the typical load factor applied to the plant on the dispatch efficiency, which translates into modest improvement of η_{dp} as the load factor is decreased (a trend even more pronounced for highly insolated locations such as as Antofagasta (depicted in Figure 5) and Phoenix (Figure S30)). Overall, the global performance of the different

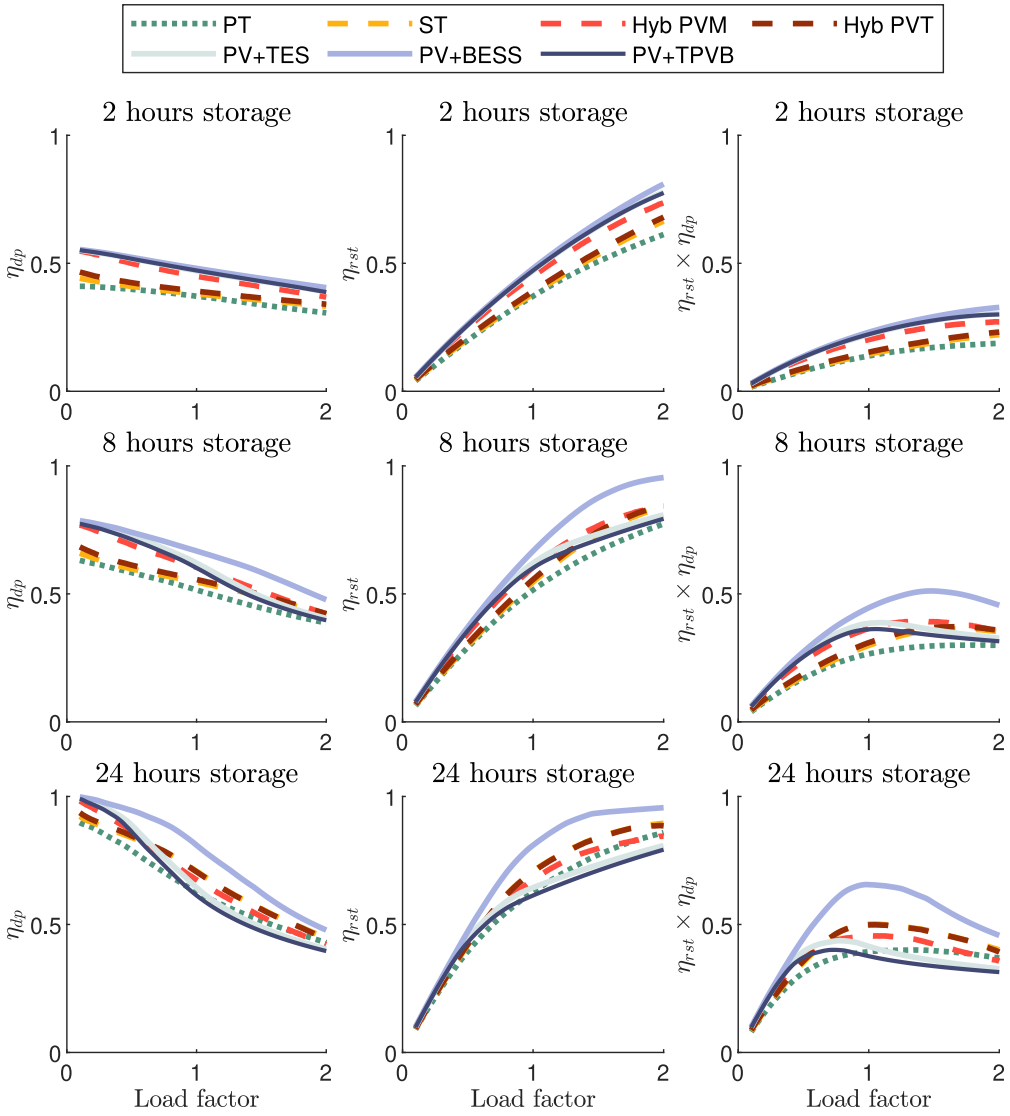

Figure 4. dispatch efficiency (left), restitution efficiency (center) and overall performance indicator (right) for the 7 solar + storage technologies in Targasonne (France)

The 3 upper figures correspond to a storage duration of 2 h, the central and lower figures respectively corresponding to 8 and 24 h of storage.

storage systems appear to be limited, with $\eta_{dp} \times \eta_{rst}$ values hardly exceeding 0.3 for large load factor values. In these conditions, the storage performance is maximized by ensuring a large energy restitution, i.e., by applying high load factors to the plant.

- For increasing values of the storage, the maximum $\eta_{dp} \times \eta_{rst}$ progressively shifts toward lower load factor values, as the result of the significant improvement in the dispatch efficiency achievable. Both the peak load factor value and the maximum associated $\eta_{dp} \times \eta_{rst}$ depend on the storage efficiency and the solar resource available (a point which can be clearly grasped from the comparison of Figures 4 and 5). For storage duration of 24 h, storage systems showing a high roundtrip efficiency (such as BESS) demonstrate peak $\eta_{dp} \times \eta_{rst}$ values of $\sim$ 0.6 and 0.8 at Targasonne and Antofagasta respectively, for load factors close to 1. Conversely, storage systems characterized by low roundtrip efficiencies (such as PV + TES or PV + TPVB) show overall storage performance barely exceeding 0.5 even for storage duration as long as 24 h. The peak load factor is offset toward lower load factors, indicating that an optimal use of the storage requires the plant to be operated at low mean power.
- Attaining dispatch efficiencies approaching 1 and satisfying the electrical demand throughout the year is possible, provided that the load factor applied to the plant is sufficiently low and the typical storage duration is high enough. However, high dispatchability is achieved at the expense of energy restitution, and highly dispatchable solar plants may thus incur large energy penalties (which translates into restitution efficiencies as low as 0.2–0.4 for load factors consistent with high dispatchabilities). This may, in turn, affect other crucial storage indicators likely to be penalized by insufficient energy restitution, such as the carbon footprint of storage or the cost of

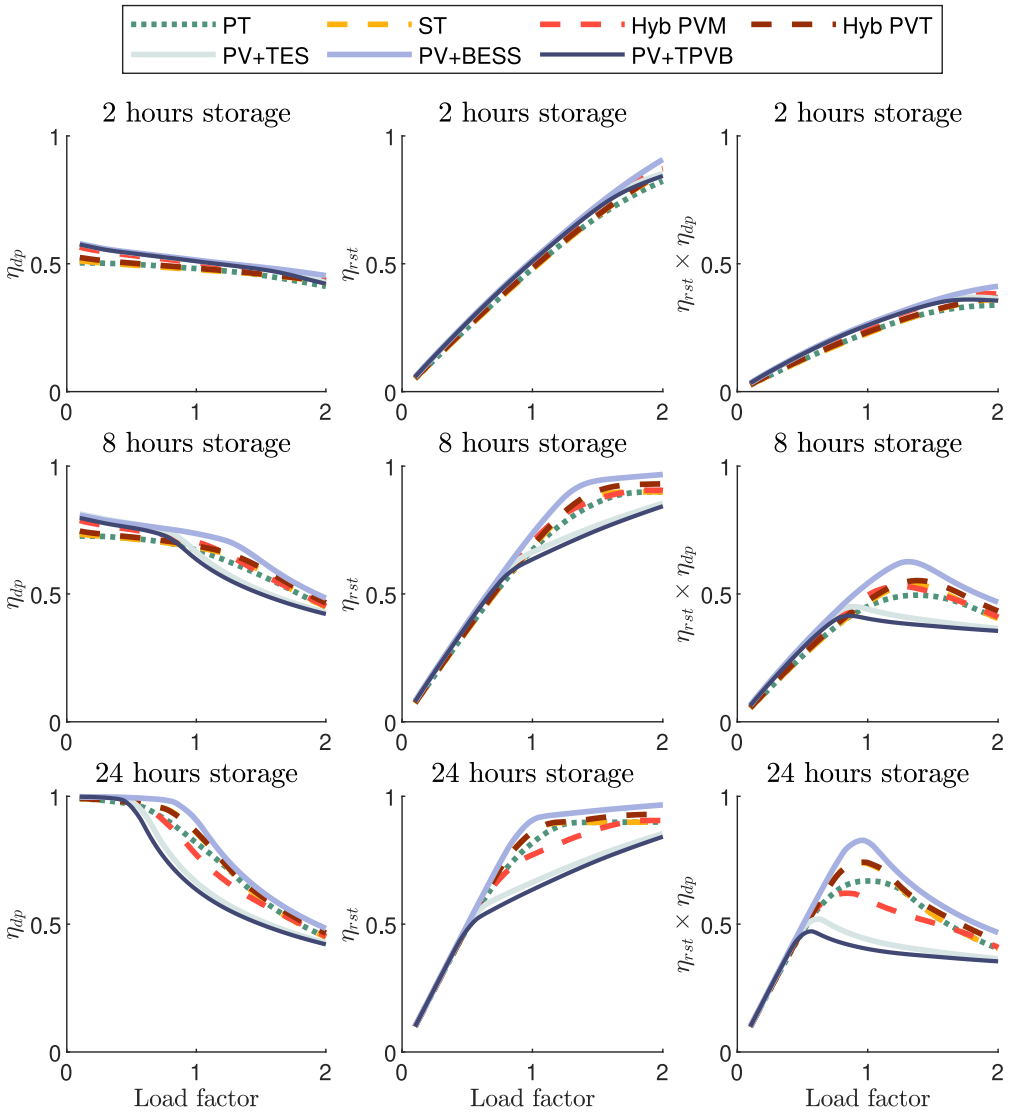

Figure 5. dispatch efficiency (left), restitution efficiency (center) and overall performance indicator (right) for the 7 solar + storage technologies in Antofagasta (Chile)

The 3 upper figures correspond to a storage duration of 2 h, the central and lower figures respectively corresponding to 8 and 24 h of storage.

the electricity delivered to the grid. This prompts the need for an economic evaluation of the different solar + storage technologies under investigation, to clarify what is the cost of dispatchability.

Evaluating the cost of dispatchability

We finally evaluate how the quest of increased dispatchability involves a penalty on the electricity cost. To do so, we estimate the LCOE for each plant under investigation. The LCOE is basically calculated as the ratio between the total costs associated with the plant operation during its lifetime, and the electrical energy delivered in the electrical network (a detailed explanation regarding the economic model used for cost calculation, as well as the economic data supporting these calculations, can be found in the supplemental information).

Cost assumptions

The estimation of the electricity cost associated with each plant under investigation requires several assumptions to be formulated.

1. The cost of the main components is essentially retrieved from NREL databases compiling theses data across US plants,[36,37] as well as from additional recent cost estimates.[38,39] These cost estimations thus do not take into account the prices disparities likely to be met

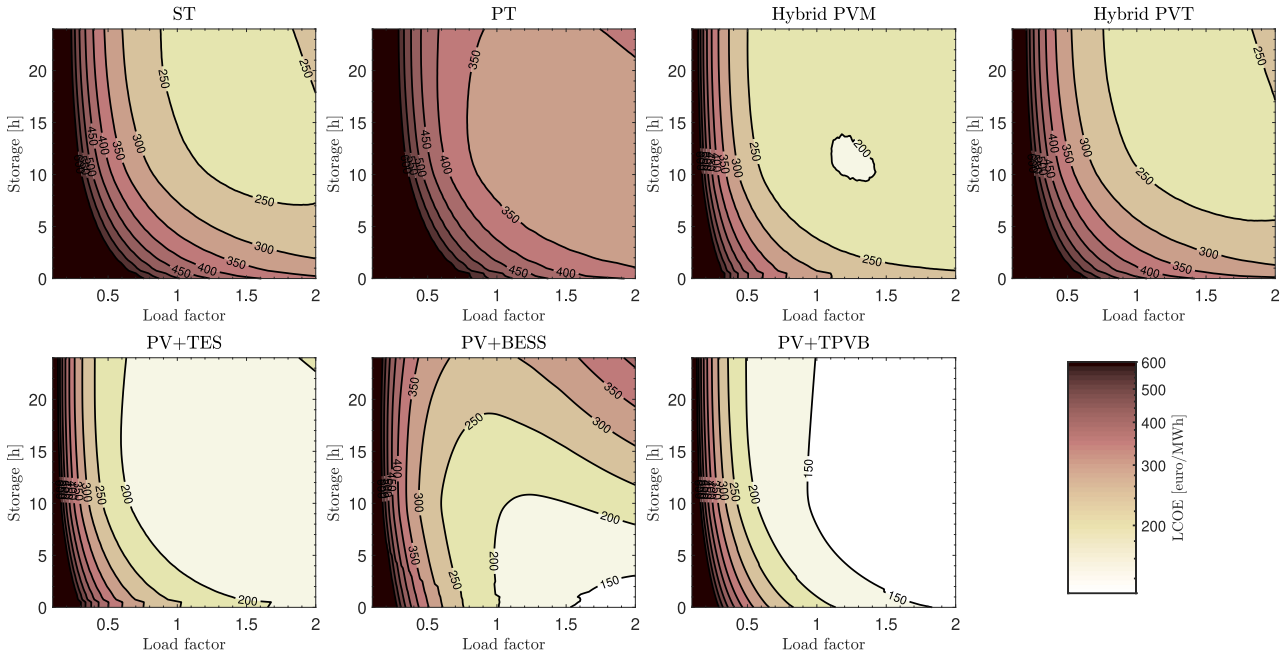

Figure 6. LCOE of the 7 approaches investigated at Targasonne, France

between different regions of the world, and more recent estimates would probably lead to minor deviations in this cost evaluation procedure. However, the temporal and spatial intervals over which the data are aggregated offers a solid basis for fair comparisons between the technologies.

2. The technological maturity of the different approaches under investigation differs significantly: while conventional PV modules are already deployed at a TW scale worldwide, both hybrid PV-CSP approaches and TPV batteries remain low TRL concepts without any short-term commercial deployment perspective. This technological gap induces at least two additional hurdles, namely 1) the costs of the key components of each hybrid approach (for instance, the PV mirrors used as heliostats in the PVM approach, the integrated PV/CSP receiver in the PVT approach, or the TPV modules used in TPV batteries) remain essentially unknown. To circumvent this obstacle, we first assume that the cost of these components is equal to the cost of comparable components in similar technologies (i.e., conventional PV modules in the case of PV mirrors and conventional CSP receivers in the case of hybrid PV/CSP integrated receivers). This assumptions will potentially induce a price bias in favor of the least mature technologies, which will be discussed in the final section of this paper 2) Some key parameters associated with the long-term operation of these plants (such as the lifetime of the main components, their degradation rates, and the *O&M* costs) cannot be retrieved nor evaluated, due to the lack of feedback regarding the real operation of these plants.

Cost evaluation

Figure 6 illustrates the levelized cost of electricity for the 7 solar + storage technologies under investigation, as a function of the load factor *f* applied to the plant, and for storage durations up to 24 h, in Targasonne, France (the corresponding LCOE curves for Antofagasta, Quito and Phoenix, are reported in Figures S31–S33, respectively).

As can be seen in Figure 6, the LCOE is basically minimized for plants operated at high load factors. However, the electricity cost dependence on storage is more subtle and is correlated with the cost structure of the different storage systems investigated. For instance, the high Cost per Energy (CPE) of batteries[40,41] incurs a cost penalty on the electricity for high storage duration: the improvement in the energy restitution is rapidly counterbalanced by the additional storage cost, which leads to a significant increase in the cost of electricity with increasing storage duration. Conversely, the integration of thermal storage offers an affordable path for better restoring the electrical energy, owing to its low CPE, and leads to a drop in LCOE for increasing storage duration. However, there is a threshold storage value (which is function of both the storage and the solar conversion technology cost) beyond which the further integration of storage does not correlate with decrease in the LCOE: the gain in the energy restitution associated with the additional integration of a storage unit does not compensate for the additional cost of this supplementary storage volume. The analysis of the curves associated with the other sites reveals that highly insolated locations (such as Antofagasta, depicted in Figure S31 and Phoenix, in Figure S33) are more favorable to CSP technologies, owing to their larger solar resource. The added value of Hybrid PV-CSP systems relative to conventional CSP technologies also appears to vanish.

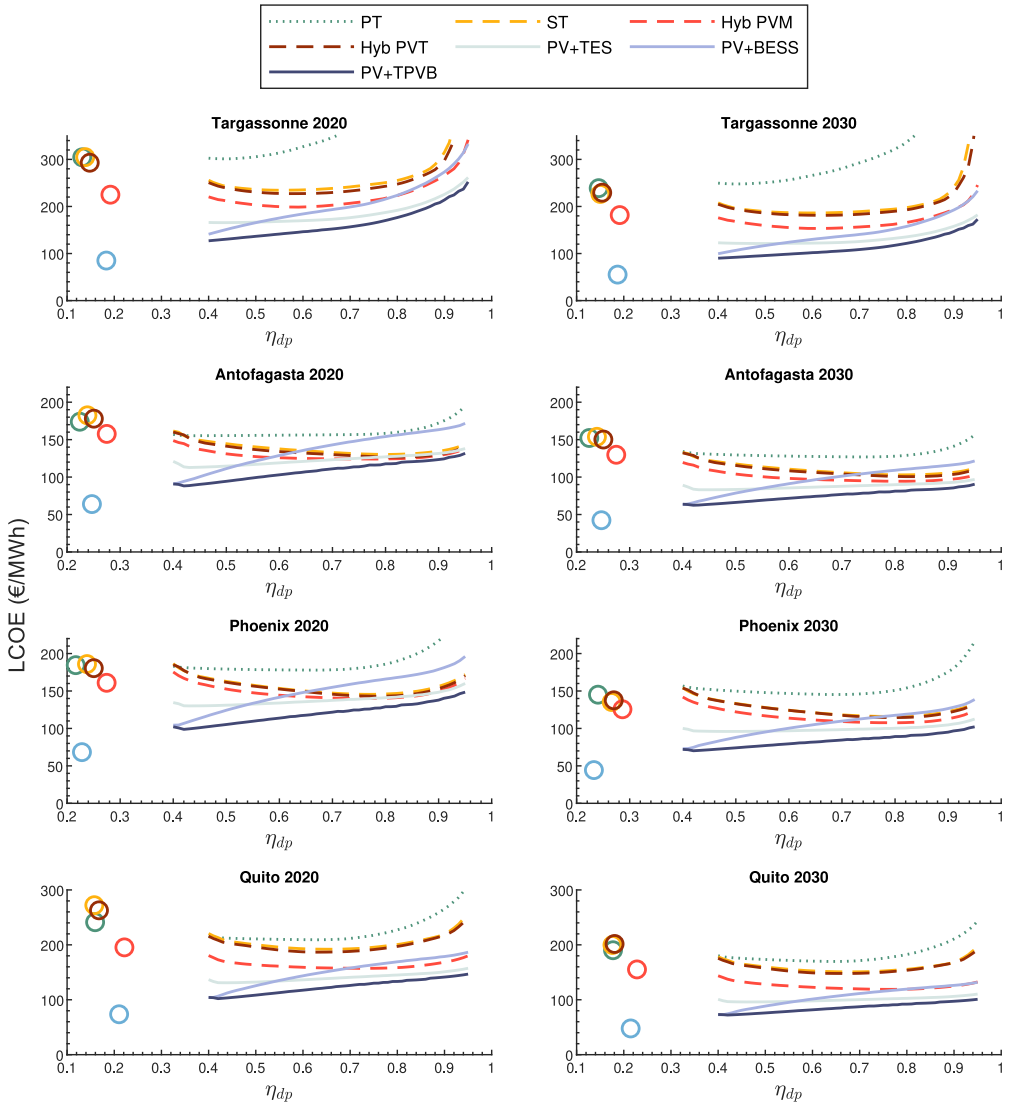

Figure 7. LCOE as a function of the dispatch efficiency η_{dp}, at Antofagasta, Phoenix, Quito, and Targasonne

The colored circles indicate the LCOE and the dispatch efficiency associated with each solar conversion technology, without any storage.

The cost penalty associated with a given demand satisfaction can be better grasped in Figure 7, showing how the LCOE varies as a function of the dispatch efficiency (these curves are deduced from the LCOE = f (η_{dp}) datapoints, and correspond to the lower boundary of the envelop encompassing them). These curves thus provide a lower bound for the LCOE achievable at any value of the dispatch efficiency.

The analysis of Figure 7 reveals several key conclusions

- As shown by the circles representing the LCOE without any storage, CSP and hybrid PV-CSP technologies are characterized by costs without storage typically between 150 and more than 300€/MWh, while PV technology shows costs typically 3 times lower than CSP. The integration of storage leads to a noticeable decrease in the cost of stored electricity in the case of CSP and hybrid systems, but to a significant increase in the cost of electricity in the case of PV. This observation highlights that the deployment of CSP plants without storage is an economic aberration given (1) the existence of an alternative technology that can deliver "non-stored" solar electricity at a significantly lower cost and (2) the noticeable decrease in the cost of CSP electricity associated with the integration of thermal storage.
- While the increase in dispatchability is associated with a steady increase in LCOE for PV + BESS, the low CPE of storage technologies involving thermal energy leads overall to much less marked variations in LCOE as a function of dispatchability. This observation is particularly valid for the most insolated sites (such as Antofagasta and Phoenix).

- A sharp increase in the LCOE can be noticed for η_{dp} exceeding ~ 0.9, due to the difficulty in fully meeting the load imposed to the plant throughout the year. As already stressed in Figure 5, achieving high dispatchability comes at the expense of energy restitution, which necessarily lead to a significant cost overrun. One should note that the η_{dp} value above which the LCOE increases sharply exceeds 0.9 for Antofagasta and Phoenix, thanks to their high solar resource, but also for Quito, despite its moderate insolation. Such a behavior can be explained by the satisfactory matching between demand and production over the year on this site.
- Despite their supposedly high costs, batteries offer an affordable alternative toward reaching moderately high dispatch efficiencies. Beyond η_{dp} of ~ 0.5–0.6, the high CPE of this storage technology prevent it to outperform thermal energy-based storage systems. The combination of PV and thermal energy storage (either TES or TPVB) appears as the most affordable option across the range of dispatch efficiencies investigated. Overall, PV + TPVB offers the most attractive economic indicators across a wide range of dispatch efficiencies, and for all the locations investigated. One should however stress that CSP technology based on solar towers constitute a relevant option for delivering affordable solar electricity with dispatch efficiencies exceeding 0.7, in the most insolated sites.
- The cost projections for 2030 show an overall decrease in costs in similar proportions for each of the technologies studied. Consequently, the superiority of one or the other of the technologies to satisfy the electric demand remains globally unchanged, whatever the considered site or the targeted dispatch efficiency. It should be noted, however, that the decreasing cost of electrochemical storage by 2030 will likely lead to a narrowing of the dispatchability range within which CSP technologies are likely to outperform PV + BESS technology.

Figure 8 summarizes how the LCOE cost structure evoluates for increasing values of the dispatchability, for the ST, PV + BESS and PV + TES technologies (the 4 other technologies have not been included in this analysis, either because of their low technological maturity, which prevents any analysis of this kind, or because of their high cost (especially for PT technology)). 3 representative values of the dispatch efficiency have been selected here, corresponding to different levels of solar electricity deployment in the electrical grid: η_{dp} = 0.5 is representative of an energy mix where solar electricity is largely complemented by other electricity sources. On the opposite, η_{dp} = 0.9 corresponds to an energy mix which is essentially driven by solar electricity. An intermediate dispatchability value (η_{dp} = 0.75) is also reported. The LCOE cost structure is shown for Targasonne (upper subfigure) and Antofagasta (lower subfigure), the figures associated with Quito and Phoenix being reported in the supplemental information (Figures S34 and S35 respectively).

Figure 8 reveals that the fraction of the LCOE associated with storage increases noticeably with dispatchability for PV + BESS, but remains modest for the 2 other technologies involving thermal storage, even for very high dispatchability values. Conversely, the cost associated with PV modules in the PV + BESS technology remains almost constant throughout the dispatchability values investigated, while it increases noticeably for PV + TES, as a consequence of the low roundtrip efficiency of the latter. As a result, decreasing the cost of electrochemical storage is a necessary condition toward lowering the price of PV + BESS electricity. On the other hand, the decrease in the PV + TES electricity cost will be mainly driven by the improvement in the storage roundtrip efficiency, and the decrease in the PV modules cost. The LCOE cost structure of the ST technology is weakly dependent on the dispatchability at Antofagasta. On the contrary, we observe a noticeable increase in the LCOE of the ST Technology at Targasonne for increasing dispatchabilities, which is mainly governed by the cost increase associated with the heliostat field and the solar receiver. Lowering the cost of these two components will thus be key toward decreasing the cost of ST electricity in the less insolated sites.

DISCUSSION

The results discussed above offer new perspectives regarding the ability of the main solar and storage technologies to meet the electrical demand over extended periods of operation. The combination of conventional PV modules together with thermal energy-based storage systems appears as the most affordable strategy to achieve high dispatchability of solar electricity at low cost. In this spirit, TPVB has recently instigated a strong interest, thanks to the very promising TPV efficiency demonstrated experimentally.[42] In addition to its potentially low storage cost, TPVB would offer a scalable storage solution, likely to be implemented over a wide range of solar plant peak powers. However, these systems still require major research and development efforts (aimed for instance at improving *thermal-to-electricity* conversion efficiency, minimizing the system losses, achieving components withstanding very high temperatures …) and cannot thus be considered today as a short-term solution for energy storage. On the contrary, the integration of regular TES in conventional PV plants constitutes a more realistic option for short-term implementation, these systems being already largely integrated in commercial CSP plants. These storage systems are less scalable than TPVB, the profitability of the turbines used for the conversion of heat into electricity being constrained by their size. However, thanks to the use of electrical energy as the source of heat, one can envision very large storage units gathering and storing the electrical energy produced by many PV plants located at distances reaching tens to hundreds of km, with only minimal transmission losses. In order to lower the CPP of these storage systems, which is currently the Achilles heel of this technology, it will be necessary to develop "high-temperature" turbines capable of efficiently converting heat at temperatures higher than those commonly encountered in CSP plants. Although CSP technology is unlikely to be the most cost-effective way to ensure increased dispatchability, it is nevertheless a promising option for ensuring a good match between demand and production in the sunniest regions of the world. Indeed, the low cost of electricity confirms that in the absence of other complementary energy sources (a situation likely to be encountered in desert regions adapted to this technology), CSP alone will probably be able to meet the electrical demand at a reasonable cost. These results also call into question the relevance of hybrid PV-CSP systems: even though hybrid PVM systems slightly outperform conventional ST plants in moderately insolated sites, the gain achieved does not allow this technology to position itself as an affordable alternative. Hybrid PVT and conventional CSP technologies show very similar

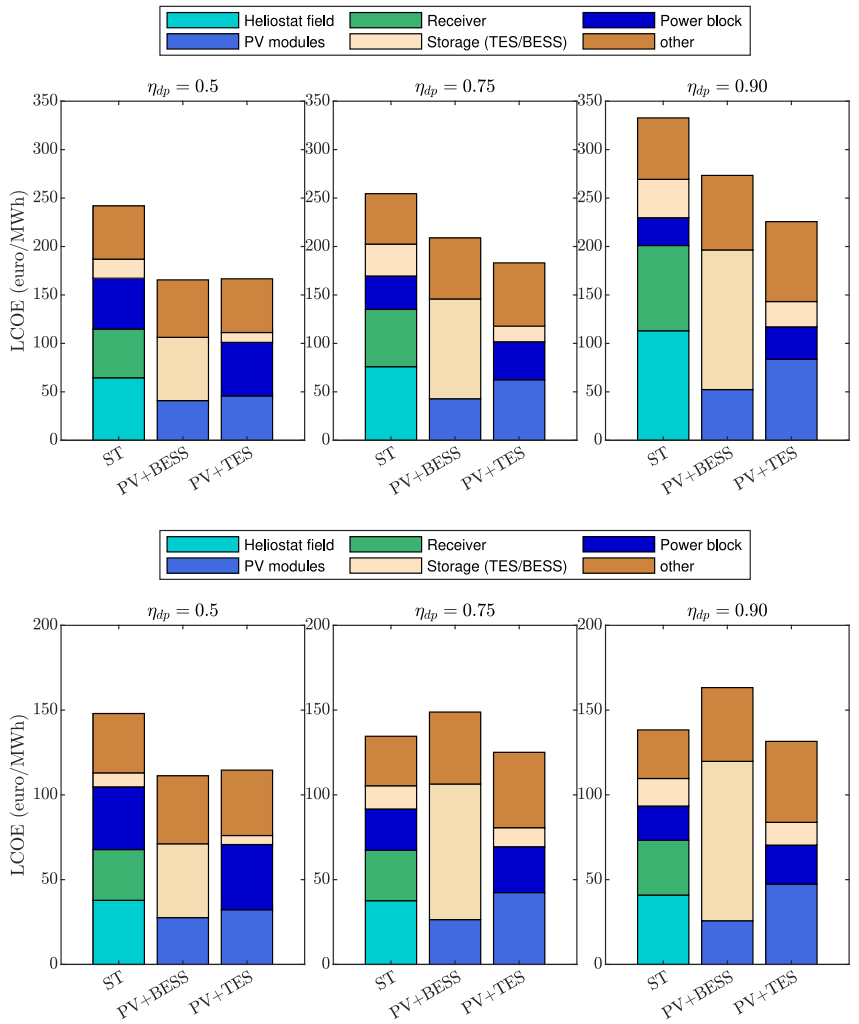

Figure 8. LCOE cost structure of the ST, PV + BESS and PV + TES technologies, for dispatch efficiency of 0.5, 0.75 and 0.90 at Targasonne (upper subfigure) and Antofagasta (lower subfigure)

behaviors, suggesting that the increased complexity of the former systems does not find any justification on some economical grounds. Finally, it should be stressed that the temporal characteristics of the plants (for instance, the distribution of unmet hours of electrical demand throughout a typical year of operation) has not been addressed here, since it is largely dependent upon operation costs (i.e., the cost associated with turbine start-up and shutdown), the financial framework governing plant operation, or the structure of the energy market. These factors will have to be taken into account when sizing solar power plants designed to meet electricity demand.

Conclusions

The management of solar electricity within the grid will have to evolve radically in the years and decades to come: at present, it is essentially injected as it goes along, without any particular concern about the adequacy between the available solar power and the demand. In this work, we have tried to evaluate the capacity of the main solar technologies to satisfy the electrical demand by considering their association with 3 different means of energy storage. In this objective, we have modeled several types of solar power plants integrating a variable storage duration, to better understand the capacity of the latter to satisfy an imposed electrical demand profile. Technical-economic indicators have been proposed and discussed, and several important conclusions can be drawn from their analysis: imposing the satisfaction of the electrical demand generates potentially significant energy losses, largely depending on the characteristics of the storage and the operating conditions imposed on the plant. There is necessarily a trade-off between energy restitution and demand satisfaction (evaluated here through *dispatchability*): the quest for high dispatchability necessarily generates additional energy losses, linked to the roundtrip efficiency of the storage system used, as well as to the mismatch between the imposed demand profile, solar electricity production, and the storage sizing. From a technical point of view, electrochemical batteries offer the best compromise between dispatchability and restitution, owing to their high

round-trip efficiency. Despite its high cost, this storage technology has the best technical and economic indicators for dispatchability efficiencies of up to 50–60 %. However, the high CPE of batteries is a major obstacle to achieving very high dispatchability at low cost. Thermal energy storage is a promising technology in the search for high dispatchability (whether conventional thermal storage or storage via TPV batteries). Its combination with PV technology generally leads to the lowest electricity costs whatever the targeted dispatch efficiencies. Despite the advantage of thermal storage, CSP technology is generally not the most economically attractive option due to the high cost of the conversion technology. However, it should be noted that this technology presents particularly interesting technical and economic indicators on the sunniest sites, where it seems to be able to meet the electrical demand on its own in the absence of a complementary energy source, and at reasonable costs. Compared to competing technologies, PV-CSP hybrid technologies do not seem to offer the technical and economic added value that would justify their deployment. Finally, it should be noted that this study is a worst-case scenario in that solar energy is judged on the basis of its ability to meet the electricity demand of a given region or country alone. In reality, it is reasonable to assume that the existence of complementary energy sources (such as wind power, hydroelectricity, etc.) will significantly reduce the need for storage to meet a given electricity demand, without altering the conclusions achieved here considering solely solar energy.

Limitations of the study

Due to the very different maturity of the technologies studied, the uncertainties associated with the costs of the main component differ significantly between technologies. For example, the cost of parabolic trough collectors or PV plants is largely documented, while the cost of thermophotovoltaic batteries remains highly speculative (in addition, the typical costs associated with the different components of each technology are time and location dependent, potentially leading to noticeable variations in the electricity cost from one location to another). The estimates provided here were based considering a peak power of 100 MW, corresponding to very large-scale power plants. One may expect the main conclusions of this work to be partly altered in the case of small or medium-size solar plants. A rigorous understanding of how the main technical and economic indicators discussed in this work change depending on the typical peak power would require a dedicated parametric study (which is not in the scope of this work). However, the size-dependence of the cost of the main components remains poorly documented for several technologies investigated here, making such an evaluation particularly cumbersome.

STAR★METHODS

Detailed methods are provided in the online version of this paper and include the following:

- KEY RESOURCES TABLE
- RESOURCE AVAILABILITY
  - Lead contact
  - Materials availability
  - Data and code availability
- NOMENCLATURE
- METHOD DETAILS
  - Solar plants
  - Storage
  - Model
  - Site selection
  - Technical models
  - General information
  - Solar collection models
  - Energy storage model
  - Economic model

SUPPLEMENTAL INFORMATION

Supplemental information can be found online at https://doi.org/10.1016/j.isci.2023.108028.

ACKNOWLEDGMENTS

The authors want to acknowledge to the Solidarity Fund for Innovative Projects (Research and Education) (FSPI) managed by the France Embassy in Equator (funded by the French Ministry for Europe and Foreign Affairs) for supporting this research.

AUTHOR CONTRIBUTIONS

Conceptualization, A.V., F.O., T.F., and A.D.; Methodology, F.O., A.V., and T.F., Software, F.O., T.F., and A.V., Validation, F.O., A.V., T.F., and A.D., Investigation, F.O., A.V., T.F., and A.D.; Writing – Original Draft: A.V.; Writing – Review and Editing: A.V., F.O., T.F., and A.D., Visualization: A.V. and F.O.

DECLARATION OF INTERESTS

The authors declare no competing interests.

Received: May 1, 2023
Revised: September 5, 2023
Accepted: September 21, 2023
Published: October 10, 2023

REFERENCES

1. PVM (2023). Record PV electricity price. https://www.pv-magazine.com/2021/04/08/saudi-arabias-second-pv-tender-draws-world-record-low-bid-of-0104-kwh/.
2. IEA (2020). Projected Costs of Generating Electricity 2020. https://www.iea.org/reports/projected-costs-of-generating-electricity-2020.
3. PVMagazine (2023). TW installation of PV. https://www.pv-magazine.com/2022/03/15/humans-have-installed-1-terawatt-of-solar-capacity/.
4. IEA (2023). Snapshot of Global PV Markets 2022. https://iea-pvps.org/snapshot-reports/snapshot-2022/.
5. Bird, L., Lew, D., Milligan, M., Carlini, E.M., Estanqueiro, A., Flynn, D., Gomez-Lazaro, E., Holttinen, H., Menemenlis, N., Orths, A., et al. (2016). Wind and solar energy curtailment: A review of international experience. Renew. Sustain. Energy Rev. *65*, 577–586. https://doi.org/10.1016/j.rser.2016.06.082.
6. Prokhorov, O., and Dreisbach, D. (2022). The impact of renewables on the incidents of negative prices in the energy spot markets. Energy Pol. *167*, 113073. https://doi.org/10.1016/j.enpol.2022.113073.
7. Hannan, M., Wali, S., Ker, P., Rahman, M.A., Mansor, M., Ramachandaramurthy, V., Muttaqi, K., Mahlia, T., and Dong, Z. (2021). Battery energy-storage system: A review of technologies, optimization objectives, constraints, approaches, and outstanding issues. J. Energy Storage *42*, 103023. https://doi.org/10.1016/j.est.2021.103023.
8. Blakers, A., Stocks, M., Lu, B., and Cheng, C. (2021). A review of pumped hydro energy storage. Prog. Energy *3*, 022003. https://doi.org/10.1088/2516-1083/abeb5b.
9. Olabi, A.G., Wilberforce, T., Abdelkareem, M.A., and Ramadan, M. (2021). Critical review of flywheel energy storage system. Energies *14*, 2159. https://doi.org/10.3390/en14082159.
10. Olabi, A., Wilberforce, T., Ramadan, M., Abdelkareem, M.A., and Alami, A.H. (2021). Compressed air energy storage systems: Components and operating parameters–a review. J. Energy Storage *34*, 102000. https://doi.org/10.1016/j.est.2020.102000.
11. Gordon, J.M., Fasquelle, T., Nadal, E., and Vossier, A. (2021). Providing large-scale electricity demand with photovoltaics and molten-salt storage. Renew. Sustain. Energy Rev. *135*, 110261. https://doi.org/10.1016/j.rser.2020.110261.
12. Shaner, M.R., Davis, S.J., Lewis, N.S., and Caldeira, K. (2018). Geophysical constraints on the reliability of solar and wind power in the united states. Energy Environ. Sci. *11*, 914–925. https://doi.org/10.1039/C7EE03029K.
13. Tong, D., Farnham, D.J., Duan, L., Zhang, Q., Lewis, N.S., Caldeira, K., and Davis, S.J. (2021). Geophysical constraints on the reliability of solar and wind power worldwide. Nat. Commun. *12*, 6146. https://doi.org/10.1038/s41467-021-26355-z.
14. Liu, G., Liu, J., Jiaqiang, E., Li, Y., Zhang, Z., Chen, J., Zhao, X., and Hu, W. (2019). Effects of different sizes and dispatch strategies of thermal energy storage on solar energy usage ability of solar thermal power plant. Appl. Therm. Eng. *156*, 14–22. https://doi.org/10.1016/j.applthermaleng.2019.04.041.
15. Pan, C.A., and Dinter, F. (2017). Combination of PV and central receiver CSP plants for base load power generation in South Africa. Sol. Energy *146*, 379–388. https://doi.org/10.1016/j.solener.2017.02.052.
16. Parrado, C., Girard, A., Simon, F., and Fuentealba, E. (2016). 2050 LCOE (levelized cost of energy) projection for a hybrid PV (photovoltaic)-CSP (concentrated solar power) plant in the Atacama desert, Chile. Energy *94*, 422–430. https://doi.org/10.1016/j.energy.2015.11.015.
17. Zurita, A., Mata-Torres, C., Cardemil, J.M., Guédez, R., and Escobar, R.A. (2021). Multi-objective optimal design of solar power plants with storage systems according to dispatch strategy. Energy *237*, 121627. https://doi.org/10.1016/j.energy.2021.121627.
18. Pilotti, L., Colombari, M., Castelli, A., Binotti, M., Giaconia, A., and Martelli, E. (2023). Simultaneous design and operational optimization of hybrid CSP-PV plants. Appl. Energy *331*, 120369. https://doi.org/10.1016/j.apenergy.2022.120369.
19. Petrollese, M., and Cocco, D. (2016). Optimal design of a hybrid CSP-PV plant for achieving the full dispatchability of solar energy power plants. Sol. Energy *137*, 477–489. https://doi.org/10.1016/j.solener.2016.08.027.
20. Gedle, Y., Schmitz, M., Gielen, H., Schmitz, P., Herrmann, U., Boura, C.T., Mahdi, Z., Caminos, R.A.C., and Dersch, J. (2022). Analysis of an integrated CSP-PV hybrid power plant. In AIP Conference Proceedings, *2445* (AIP Publishing LLC), 030009. https://doi.org/10.1063/5.0086236.
21. Liu, T., Yang, J., Yang, Z., and Duan, Y. (2022). Techno-economic feasibility of solar power plants considering PV/CSP with electrical/thermal energy storage system. Energy Convers. Manag. *255*, 115308. https://doi.org/10.1016/j.enconman.2022.115308.
22. Starke, A.R., Cardemil, J.M., Escobar, R.A., and Colle, S. (2016). Assessing the performance of hybrid CSP + PV plants in northern Chile. Sol. Energy *138*, 88–97. https://doi.org/10.1016/j.solener.2016.09.006.
23. Starke, A.R., Cardemil, J.M., Escobar, R., and Colle, S. (2018). Multi-objective optimization of hybrid CSP + PV system using genetic algorithm. Energy *147*, 490–503. https://doi.org/10.1016/j.energy.2017.12.116.
24. Sumayli, H., El-Leathy, A., Danish, S.N., Al-Ansary, H., Almutairi, Z., Al-Suhaibani, Z., Saleh, N.S., Saeed, R.S., Alswaiyd, A., Djajadiwinata, E., and Alaqel, S. (2023). Integrated CSP-PV hybrid solar power plant for two cities in Saudi Arabia. Case Stud. Therm. Eng. *44*, 102835. https://doi.org/10.1016/j.csite.2023.102835.
25. Bravo, R., Ortiz, C., Chacartegui, R., and Friedrich, D. (2021). Multi-objective optimisation and guidelines for the design of dispatchable hybrid solar power plants with thermochemical energy storage. Appl. Energy *282*, 116257. https://doi.org/10.1016/j.apenergy.2020.116257.
26. Iñigo-Labairu, J., Dersch, J., and Schomaker, L. (2022). Integration of CSP and PV power plants: Investigations about synergies by close coupling. Energies *15*, 7103. https://doi.org/10.3390/en15197103.
27. Riffelmann, K.-J., Weinrebe, G., and Balz, M. (2022). Hybrid CSP-PV plants with integrated thermal storage. In AIP Conference Proceedings, *2445* (AIP Publishing LLC), 030020. https://doi.org/10.1063/5.0086610.
28. Cox, J.L., Hamilton, W.T., and Newman, A.M. (2023). Parametric analysis on optimized design of hybrid solar power plants. Sol. Energy *252*, 195–217. https://doi.org/10.1016/j.solener.2023.01.016.
29. Jorgenson, J., Mehos, M., and Denholm, P. (2016). Comparing the net cost of CSP-TES to PV deployed with battery storage. In AIP Conference Proceedings, *1734* (AIP Publishing LLC), 080003. https://doi.org/10.1063/1.4949183.
30. Braff, W.A., Mueller, J.M., and Trancik, J.E. (2016). Value of storage technologies for wind and solar energy. Nat. Clim. Change *6*, 964–969. https://doi.org/10.1038/nclimate3045.
31. Budischak, C., Sewell, D., Thomson, H., Mach, L., Veron, D.E., and Kempton, W. (2013). Cost-minimized combinations of wind power, solar power and electrochemical storage, powering the grid up to 99.9% of the time. J. Power Sources *225*, 60–74. https://doi.org/10.1016/j.jpowsour.2012.09.054.
32. Ziegler, M.S., Mueller, J.M., Pereira, G.D., Song, J., Ferrara, M., Chiang, Y.-M., and Trancik, J.E. (2019). Storage requirements and costs of shaping renewable energy toward grid decarbonization. Joule *3*, 2134–2153. https://doi.org/10.1016/j.joule.2019.06.012.
33. Arbabzadeh, M., Sioshansi, R., Johnson, J.X., and Keoleian, G.A. (2019). The role of energy storage in deep decarbonization of electricity production. Nat. Commun. *10*, 3413. https://doi.org/10.1038/s41467-019-11161-5.
34. Dowling, J.A., Rinaldi, K.Z., Ruggles, T.H., Davis, S.J., Yuan, M., Tong, F., Lewis, N.S., and Caldeira, K. (2020). Role of long-duration energy storage in variable renewable

electricity systems. Joule *4*, 1907–1928. https://doi.org/10.1016/j.joule.2020.07.007.
35. Pellow, M.A., Emmott, C.J.M., Barnhart, C.J., and Benson, S.M. (2015). Hydrogen or batteries for grid storage? A net energy analysis. Energy Environ. Sci. *8*, 1938–1952. https://doi.org/10.1039/C4EE04041D.
36. Feldman, D., Ramasamy, V., Fu, R., Ramdas, A., Desai, J., and Margolis, R.U.S. (2020). Solar photovoltaic system and energy storage cost benchmark: Q1 2020. Tech. Rep.. www.nrel.gov/publications
37. Turchi, C.S., Boyd, M., Kesseli, D., Kurup, P., Mehos, M., Neises, T., Sharan, P., Wagner, M.J., and Wendelin, T. (2019). CSP Systems Analysis - Final Project Report. Tech. Rep.. www.nrel.gov/publications
38. Boukelia, T.E., Bouraoui, A., Laouafi, A., Djimli, S., and Kabar, Y. (2020). 3E (Energy-Exergy-Economic) comparative study of integrating wet and dry cooling systems in solar tower power plants. Energy *200*. https://doi.org/10.1016/j.energy.2020.117567.
39. Giostri, A., Binotti, M., Sterpos, C., and Lozza, G. (2020). Small scale solar tower coupled with micro gas turbine. Renew. Energy *147*, 570–583. https://doi.org/10.1016/j.renene.2019.09.013.
40. Amy, C., Seyf, H.R., Steiner, M.A., Friedman, D.J., and Henry, A. (2019). Thermal energy grid storage using multi-junction photovoltaics. Energy Environ. Sci. *12*, 334–343. https://doi.org/10.1039/C8EE02341G.
41. Datas, A., López-Ceballos, A., López, E., Ramos, A., and del Cañizo, C. (2022). Latent heat thermophotovoltaic batteries. Joule *6*, 418–443. https://doi.org/10.1016/j.joule.2022.01.010.
42. LaPotin, A., Schulte, K.L., Steiner, M.A., Buznitsky, K., Kelsall, C.C., Friedman, D.J., Tervo, E.J., France, R.M., Young, M.R., Rohskopf, A., et al. (2022). Thermophotovoltaic efficiency of 40. Nature *604*, 287–291. https://doi.org/10.1038/s41586-022-04473-y.
43. Perl, E.E., Simon, J., Geisz, J.F., Lee, M.L., Friedman, D.J., and Steiner, M.A. (2016). Measurements and Modeling of III-V Solar Cells at High Temperatures up to 400 °C. IEEE J. Photovoltaics *6*, 1345–1352. https://doi.org/10.1109/JPHOTOV.2016.2582398.
44. Perl, E.E., Simon, J., Friedman, D.J., Jain, N., Sharps, P., McPheeters, C., Sun, Y., Lee, M.L., and Steiner, M.A. (2018). Al) GaInP/GaAs tandem solar cells for power conversion at elevated temperature and high concentration. IEEE J. Photovoltaics *8*, 640–645. https://doi.org/10.1109/JPHOTOV.2017.2783853.
45. Ziegler, M.S., and Trancik, J.E. (2021). Re-examining rates of lithium-ion battery technology improvement and cost decline. Energy Environ. Sci. *14*, 1635–1651. https://doi.org/10.1039/D0EE02681F.
46. Pelay, U., Luo, L., Fan, Y., Stitou, D., and Rood, M. (2017). Thermal energy storage systems for concentrated solar power plants. Renew. Sustain. Energy Rev. *79*, 82–100. https://doi.org/10.1016/j.rser.2017.03.139.
47. da Silva Lima, L., Quartier, M., Buchmayr, A., Sanjuan-Delmás, D., Laget, H., Corbisier, D., Mertens, J., and Dewulf, J. (2021). Life cycle assessment of lithium-ion batteries and vanadium redox flow batteries-based renewable energy storage systems. Sustain. Energy Technol. Assessments *46*, 101286. https://doi.org/10.1016/j.seta.2021.101286.
48. Reilly, H.E., and Kolb, G.J. (2001). An evaluation of molten-salt power towers including results of the solar two project. Tech. Rep. Sandia Natl. Lab. (SNL-NM).
49. Kelsall, C.C., Buznitsky, K., and Henry, A. (2021). Technoeconomic analysis of thermal energy grid storage using graphite and tin. Preprint at arXiv. https://doi.org/10.48550/arXiv.2106.07624.
50. NSRDB (2023). National Solar Radiation Database. https://nsrdb.nrel.gov/.
51. PVSyst (2023). PVSyst. https://www.pvsyst.com/.
52. EIA (2023). Energy Information Administration. https://www.eia.gov/electricity/gridmonitor/dashboard/custom/pending.
53. CEN (2023). Coordinador Eléctrico Nacional, Demanda Programada. https://www.coordinador.cl/operacion/graficos/operacion-programada/demanda-programada/.
54. RTE (2023). Open Data Réseaux Energies. https://opendata.reseaux-energies.fr/.
55. CNELEP (2023). Corporación Nacional de Electricidad. https://www.cnelep.gob.ec.
56. Reda, I., and Andreas, A. (2004). Solar position algorithm for solar radiation applications. Sol. Energy *76*, 577–589.
57. Wagner, M.J., and Wendelin, T. (2018). Solarpilot: A power tower solar field layout and characterization tool. Sol. Energy *171*, 185–196.
58. Wei, X., Lu, Z., Wang, Z., Yu, W., Zhang, H., and Yao, Z. (2010). A new method for the design of the heliostat field layout for solar tower power plant. Renew. Energy *35*, 1970–1975.
59. Wei, X., Herbst, A., Ma, D., Aiken, J., and Li, L. (2011). Tracking and ray tracing equations for the target-aligned heliostat for solar tower power plants. J. Proteome Res. *10*, 2687–2702.
60. Ganapati, V., Xiao, T.P., and Yablonovitch, E. (2016). Ultra-efficient thermophotovoltaics exploiting spectral filtering by the photovoltaic band-edge. Preprint at arXiv. https://doi.org/10.48550/arXiv.1611.03544.
61. Valenzuela, L., López-Martín, R., and Zarza, E. (2014). Optical and thermal performance of large-size parabolic-trough solar collectors from outdoor experiments: A test method and a case study. Energy *70*, 456–464.
62. Sharma, V., Nayak, J., and Kedare, S. (2013). Shading and available energy in a parabolic trough concentrator field. Sol. Energy *90*, 144–153.
63. Wagner, M.J., and Gilman, P. (2011). Technical manual for the sam physical trough model. Tech. Rep. Natl. Renew. Energy Lab. (NREL).
64. Harrigan, R.W. (1981). Handbook for the conceptual design of parabolic trough solar energy systems process heat applications. Tech. Rep. Sandia Natl. Lab. (SNL-NM).
65. Branz, H.M., Regan, W., Gerst, K.J., Borak, J.B., and Santori, E.A. (2015). Hybrid solar converters for maximum exergy and inexpensive dispatchable electricity. Energy Environ. Sci. *8*, 3083–3091.
66. IRENA (2015). Solar power spatial planning techniques. In Global Atlas Training on Planning the Renewable Energy Transition Using Solar and Wind Maps (IRENA).
67. Gilman, P. (2015). Sam photovoltaic model technical reference. Tech. Rep. Natl. Renew. Energy Lab. (NREL).
68. Goswami, D.Y., Stefanakos, E.K., Hassan, A.Y., and Collis, W.J. (1989). Effect of row-to-row shading on the output of flat-plate south-facing photovoltaic arrays. J. Sol. Energy Eng. *111*, 257–259.
69. Deline, C., Dobos, A., Janzou, S., Meydbray, J., and Donovan, M. (2013). A simplified model of uniform shading in large photovoltaic arrays. Sol. Energy *96*, 274–282.
70. Appelbaum, J., and Bany, J. (1979). Shadow effect of adjacent solar collectors in large scale systems. Sol. Energy *23*, 497–507.
71. Murray, D. (2012). Small-scale Solar Central Receiver System Design and Analysis.
72. Zeitouny, J., Lalau, N., Gordon, J.M., Katz, E.A., Flamant, G., Dollet, A., and Vossier, A. (2018). Assessing high-temperature photovoltaic performance for solar hybrid power plants. Sol. Energy Mater. Sol. Cell. *182*, 61–67.
73. Green, M.A., Dunlop, E.D., Siefer, G., Yoshita, M., Kopidakis, N., Bothe, K., and Hao, X. (2023). Solar cell efficiency tables (version 61). Prog. Photovoltaics *31*, 3–16. https://doi.org/10.1002/pip.3646.
74. Shockley, W., and Queisser, H.J. (1961). Detailed balance limit of efficiency of p-n junction solar cells. J. Appl. Phys. *32*, 510–519.
75. Silverman, T.J., Deceglie, M.G., Marion, B., Cowley, S., Kayes, B., and Kurtz, S. (2013). Outdoor performance of a thin-film gallium-arsenide photovoltaic module. In 2013 IEEE 39th Photovoltaic Specialists Conference (PVSC) (IEEE), pp. 0103–0108.
76. Kafle, B., Goraya, B.S., Mack, S., Feldmann, F., Nold, S., and Rentsch, J. (2021). Topcon–technology options for cost efficient industrial manufacturing. Sol. Energy Mater. Sol. Cell. *227*, 111100.
77. Duffie, J.A., Beckman, W.A., and Blair, N. (2020). Solar Engineering of Thermal Processes, Photovoltaics and Wind (John Wiley & Sons).
78. Kebede, A.A., Kalogiannis, T., Van Mierlo, J., and Berecibar, M. (2022). A comprehensive review of stationary energy storage devices for large scale renewable energy sources grid integration. Renew. Sustain. Energy Rev. *159*, 112213.
79. Ramasamy, V., Feldman, D., Desai, J., and Margolis, R. (2021). Us solar photovoltaic system and energy storage cost benchmarks: Q1 2021. Tech. Rep. Natl. Renew. Energy Lab. (NREL).
80. Seong, W.M., Park, K.-Y., Lee, M.H., Moon, S., Oh, K., Park, H., Lee, S., and Kang, K. (2018). Abnormal self-discharge in lithium-ion batteries. Energy Environ. Sci. *11*, 970–978.

STAR★METHODS

KEY RESOURCES TABLE

REAGENT or RESOURCE	SOURCE	IDENTIFIER
Software and algorithms	OSF Home	https://doi.org/10.17605/OSF.IO/ADQ6M
SolarPilot	NREL	https://www.nrel.gov/csp/solarpilot.html
Matlab	MathWorks	https://la.mathworks.com/products/matlab.html

RESOURCE AVAILABILITY

Lead contact

Further information and request for resources should be directed to and will be fulfilled by the lead contact, Alexis Vossier (alexis.vossier@promes.cnrs.fr).

Materials availability

Not applicable.

Data and code availability

- Actual and future costs of the components were retrieved from multiple sources detailed in Appendix A.
- All original code has been deposited at OSF Home and is publicly available as of the date of publication. DOIs are listed in the key resources table.
- Any additional information required to reanalyze the data reported in this paper is available from the lead contact upon request.

NOMENCLATURE

BESS Battery Energy Storage System
BL Base Load
CAES Compressed-Air Energy Systems
CPE Cost Per Energy
CSP Concentrated Solar Power
DNI Direct Normal Incidence
E_g electronic bandgap eV
ED Electrical Demand
GHI Global Horizontal Irradiance
LCOE Levelized Cost Of Electricity
LF Linear Fresnel
LFP Lithium Ferrophosphate
PHS Pumped Hydro Energy Storage
PT Parabolic Trough
PV Photovoltaic
PVM Photovoltaic Mirror
PVT Photovoltaic Topping
SAM System Advisor Model
SD Solar Dish
ST Solar Tower
t time (*hour*)
TES Thermal Energy System
TL Tracking Load
TMY Typical Meteorological Year
TPV Thermophotovoltaic
TPVB Thermophotovoltaic Batteries
TRL Technology Readiness Level
VRE Variable Renewable Energy

Subscripts

max maximum

METHOD DETAILS

Solar plants

The main *solar-to-power* technologies investigated can be subdivided here into 3 main categories, based on their underlying physical principles:

- *Photovoltaic (PV)* plants involve a direct conversion of sunlight into electricity using PV modules. This solar technology currently holds the lion's share among the *solar-to-electricity* conversion technologies, owing to its simplicity and low cost.
- *Concentrated Solar Power (CSP)* plants are based on the indirect conversion of solar energy, first into heat, then into mechanical work, and finally into electricity. Despite their higher complexity relative to PV systems, these systems offer the inherent advantage of storing energy as heat using low-cost TES, and are often mentioned as promising candidates for extending the dispatchability of solar power at a reasonable cost. Among the four CSP technologies currently used (*i.e.* Solar Tower (ST), Parabolic Trough (PT), Linear Fresnel (LF) and Solar Dishes (SD)), two are considered in this work, namely 1) Parabolic Trough technology, where sunlight is concentrated onto an absorber tube via parabolic troughs reflectors mounted on 1-axis tracking systems. These systems currently represent the most largely deployed CSP technology worldwide ($\sim 2/3$ of the total CSP power) 2) Solar Tower technology, where sunlight is concentrated onto a receiver located at the top of a tower, after reflection on a heliostat field. ST technology is known for showing the largest cost-reduction potential among the different CSP technologies.
- *Hybrid PV/CSP* technologies, involve the combination of the two previous technologies. *Non-compact* hybrid power plants imply two PV and CSP plants built close to one another, and operated in concert to mitigate the variability of the solar resource. Conversely, *compact* hybrid power plants are based on the amalgamation of the two technologies into one single plant, and involve some specific PV components to be integrated into conventional CSP plants. Here, two different hybrid approaches were evaluated: 1) *PV Mirror* plants (identified as *hybrid PVM* throughout the text) require the mirrors of conventional heliostats to be replaced by semi-reflecting PV modules acting both as PV converters for highly energetic photons ($E > E_g$) and reflectors for below-bandgap photons ($E < E_g$). *PVM* plants theoretically allow a better use of the solar resource, first owing to the combination of two complementary solar converters, second because of the use of the diffuse radiation (which is commonly lost in conventional CSP plants). 2) *PV Topping* (denoted here as *hybrid PVT*) plants involve an integrated PV-CSP receiver where PV cells act both as PV converters and solar absorber. The high operating temperature required to efficiently run the power block implies PV cells operated at temperature levels of hundreds of degrees, exceeding by far the characteristic temperature for which conventional PV cells are commonly designed (i.e. 25 $^{\circ}C$). Despite being highly speculative today, this approach would lower thermalisation losses by better harnessing the residual heat. Recent experimental reports demonstrated that PV cells based on $III-V$ materials could withstand temperature levels consistent with this approach.[43,44]

Storage

Threes storage technologies are evaluated and compared in this work:

- *Electrochemical storage* (referred here as *BESS*) is commonly seen as one of the most obvious option for solar electricity storage, owing to its simplicity, stability, and high roundtrip efficiency. Li-ion and LFP (lithium ferrophosphate) BESS experienced a noticeable price decrease in the last decades, with a 97 % drop in price since its commercial introduction in 1991.[45] Despite these dramatic cost reductions, the price of electrochemical storage still represent a major hurdle to the massive deployment of this technology, with storage cost typically exceeding 200 USD/kWh in 2020.
- *Thermal Energy Storage* is based upon changing the temperature of a medium either by heating or cooling it. Thermal energy is then stored under the form of sensible heat (if the thermal energy is stored as a temperature difference inside a medium) or latent heat (if the storage of thermal energy involves a phase change of the storage medium).[46] Heat storage is a cost-effective storage option for solar technologies involving heat as an energy vector (such as CSP and hybrid PV/CSP systems), and has also been suggested recently as a promising storage technology for conventional PV modules or wind energy systems, via *power to heat to power* conversion.[11]
- *Thermophotovoltaic Batteries* have recently been suggested as an original and promising way to store energy.[40,41] These systems basically involve the radiation emitted by a high-temperature emitter to be absorbed by TPV cells surrounding it. The use of multi-junction TPV cells incorporating efficient back reflectors has been shown to be a key condition toward effectively converting the incident radiation, and sending back the low-energy photons to the emitter.[42] Despite their low technological maturity in comparison with the other storage technologies considered in this work, we include TPV batteries as a candidate technology owing to its potentially low cost (large-scale deployment of TPVB technology was shown to lead to storage costs that could be as low as 10 $\$/kWh$[41]).

The main storage assumptions are summarized in the following table.

BESS	
Storage temperature	ambient
Charge/discharge efficiency (electrical)	0.96
Lifetime	3000 cycles[47]
TRL	9
TES	
Storage temperature	560 ° C (400 ° C for the hybrid PVT approach)
Charge/discharge efficiency (thermal)	1
Lifetime	30 years[48]
TRL	7
TPVB	
Storage temperature	2000 ° C
Charge/discharge efficiency (thermal)	1
Lifetime	> 30 years[49]
TRL	3

Model

The comparison of solar technologies based on different operating principles, characterized by different land footprints, and using different types of solar resources (i.e. DNI, GHI) is fundamentally intricate and requires some operational assumptions to be formulated. We base our analysis on large-scale solar power plants characterized by peak power output of typically 100 MW: this choice is guided by the size-dependence of some key components costs (such as the turbines used in CSP technology) which could impede any fair comparisons between technologies demonstrating different scale cost reduction trends. By selecting large scale solar plants, we *a-priori* minimize the scale-cost biases between the different technologies under investigation. Each technology is evaluated on the basis of specific *optical-thermal-electrical* models providing the different energy flows with a time-step of 1 hour. These models were validated by comparing their outcome with those of dedicated softwares, such as the System Advisor Model (SAM) for CSP plants and PVsyst for PV plants. The relative difference between these two families of model was shown to be lower than 5 %. The core assumption of our benchmark study lies on the collection area of each technology investigated, which is assumed to be identical to the collection area required to satisfy a peak power output of typical 100 MW_e ST plant. The typical collection area necessary to fulfill this condition is calculated for each site, and serves as a reference value for the calculation of the electrical power generated by the different solar technologies studied. The next table summarizes the main operational parameters for each plant under investigation, and a detailed description of the physical model used for each technology is provided below supplemental information.

Site selection

The ability of solar energy to fulfill a particular electrical demand profile is likely to vary noticeably depending on several key parameters, namely:

1. *the solar resource*: Both the short-term and the seasonal availability of solar energy may affect the potential of solar plants to satisfy a given electrical demand as well as the need for energy storage.

	ST	PT	Hyb. PVM	Hyb. PVT	PV
Collection area [m^2]	≈1 300 000				
Solar ressource	DNI	DNI	GHI[a]	DNI	GHI
Storage type	TES	TES	TES	TES	TES/BESS/TPVB
PV technology	x	x	c-Si	GaAs	c-Si
PV efficiency	x	x	0,197	$\eta_{PV,PVT}(X,T)$ [b]	0,197

(*Continued on next page*)

Continued

	ST	PT	Hyb. PVM	Hyb. PVT	PV
Power block efficiency	42.8	36.8	42.8	37.3	x
Land occupation [m^2 *land*/ m^2 *col.*]	6.5	5.2	6.5	6.5	4.9
Operating temperature [°*C*]	560	390	560	400	25

aThe fraction of GHI absorbed by the PVM modules is calculated as a function of the heliostat orientation (see appendix).
bThe conversion efficiency is calculated as a function of both the temperature (400 ° C) and the solar flux impinging the receiver (see appendix).

2. *the electrical demand profile*: the satisfaction of the electrical load may change depending on the electrical profile imposed to the solar plant (i.e. constant or variable electrical load). In particular, the degree to which the electrical demand is matched to the solar resource availability may affect noticeably the storage volume requested upon reaching a given dispatchability level.
3. *the storage capabilities*: the ability of a particular configuration of solar plant to fulfill the electrical demand will logically be a function of the amount of energy stored.

To better grasp the ability of solar power to fulfill the electrical demand, we thus select four locations characterized by moderate-to-high solar resource and showing different electrical demand profiles along the year, namely Targasonne (France), Quito (Equator), Phoenix (USA) and Antofagasta (Chile). The hourly solar irradiation profiles at Antofagasta, Phoenix and Quito are retrieved from the National Solar Radiation Database,[50] while the corresponding data for Targasonne were retrieved from PVSyst.[51] We select TMY values, aggregating hourly data representative of the median weather conditions over a multi-year period. Each location is characterized by a different combination of solar resource/electrical demand profile: Antofagasta and Phoenix both show very high solar resources with daily DNI values exceeding 7 $kWh/m^2/day$. On the contrary, Quito and Targasonne are characterized by moderate daily DNI values, with an important diffuse solar resource in the case of Quito (which translates into a ratio DNI/GHI <1). The seasonal variations of the solar resource appear to be significantly more pronounced in Targasonne and Phoenix, due to their higher latitude, as well as their characteristic climatic conditions. The hourly electrical demand profiles at the national level are taken from[52–54] (respectively for USA, Chile and France). The data for Equator were directly retrieved from the national electricity supplier.[55] The electrical demand profile shows smooth variations throughout the year in Ecuador (Quito) and Chile (Antofagasta), while significant fluctuations of the electrical demand can be observed in the other two sites, with a peak-demand in Winter in the case of France, and in Summer in the case of the USA. The following table summarizes the main characteristics of the 4 sites investigated in this study.

	Antofagasta	Phoenix	Quito	Targasonne
Country	Chile	USA	Ecuador	France
Latitude (°)	-23.4	33.4	-0.2	42.5
Longitude (°)	-70.4	-112.1	-78	2
Elevation (m)	40	330	2800	1600
GHI ($kWh/m^2/day$)	6.55	5.80	5.70	4.30
DNI ($kWh/m^2/day$)	7.42	7.25	5.26	4.83
DNI/GHI	1.13	1.25	0.92	1.12

Technical models

In the following sections, the operational principles pertaining to each solar and energy storage (ES) technology, are described. The 7 different couples of technologies are:

- "Solar Tower" (ST);
- hybrid "Photovoltaic Mirrors" (PVM);
- hybrid "Photovoltaic Topping" (PVT);
- "Parabolic Troughs" (PT);
- "Photovoltaic with Batteries Energy Storage System" (PV-BESS);
- "Photovoltaic with Thermal Energy Storage" (PV-TES);
- "Photovoltaic with Thermophotovoltaic batteries" (PV-TPVB).

General information

Each model was designed assuming similar collection area, the Solar Tower (ST) heliostat field surface serving as the reference collector area. The reference heliostat field design have been generated using SolarPilot for each site under investigation. The models comprise three

distinct algorithms. First, the electrical power generated by each plant is calculated for each timestep over a typical year of operation. A second algorithm is then used to evaluate the electrical energy effectively injected in the grid, together with the energy stored in the storage units to which the different solar technologies are associated. The global techno-economic indicators are finally computed and compared using a third algorithm.

Solar collection models

Weather and position of the sun in the sky

Each model uses as an input a weather file corresponding to one of the 4 locations studied (i.e. Quito in Equator, Phoenix in the United States of America, Antofagasta in Chile and Targasonne in France), retrieved from the the National Solar Radiation Database[50] (Quito, Phoenix, Antofagasta) and from PVSyst database (Targasonne).[51]

For each timestep of the simulation, the Sun's Elevation and Azimuth angles, *El* and *Az*, are calculated using the *SunposCalc algorithm* (NREL).[56] Note that this algorithm uses the astronomy convention for the Azimuth, *i.e.* clockwise from North, however, the anticlockwise convention (*i.e.* anticlockwise from South, commonly used in the solar energy community) was selected here, and the sun's position was thus translated following this convention. The solar position will be used to compute the heliostats position in the next part of the model.

Solar field model (used by ST, PVT and PVM models)

In the solar field model, the incident solar flux is reflected by the heliostat field toward the 1200 m^2 thermal receiver, located at the top of the 195 m tower. The sizing of the heliostat field was performed using the SolarPilot software developed by NREL,[57] using the appropriate meteorological files as inputs, and without further modification of the basic parameters. Thus, the generated heliostat fields (unit area: S_{hel} = 148.84 m^2;), *cf.* Figure S1, correspond to a design thermal power of 670 MW, for a DNI value at the design point of 950 $W.m^{-2}$. The collection area of the heliostat fields vary slightly between locations, from 1,251,874 m^2 (Phoenix) to 1,275,840 m^2 (Quito), inducing a maximum relative difference of 2 %. Note that these areas are comparable to those of typical ST plants (such as Crescent Dunes).

The *x* and *y* positions of the heliostats are retrieved from the *SolarPilot* simulations (the bottom of the tower being the origin, *x* and *y* respectively holding positive values towards East and North), as well as their tilt angle β_{hel}, their shading efficiency $\eta_{shadowing}$ and their blocking efficiency $\eta_{blocking}$ for each hour of the year. These data allow the calculation of the heliostat surface fraction effectively used to reflect the sun towards the receiver at each time step.

The incidence angle of the solar rays on the heliostat $\theta_{i,hel}$ (*i.e.* the angle formed between the solar rays and the normal to the heliostat), is deduced from Equation 6,[58,59]

$$\cos(\theta_{i,hel}) = \frac{\sqrt{2}}{2}\cdot\sqrt{(\sin(El)\cdot\cos(\lambda) - \cos(\theta_h - Az)\cdot\cos(El)\cdot\sin(\lambda)+1)} \quad \text{(Equation 6)}$$

where λ is the angle between 1) the line passing through the top of the tower and the center of the heliostat and 2) the vertical line passing through the tower, see Equation 7,

$$\lambda = \arctan\left(\frac{d_{h-t}}{z_{tower}}\right) = \arctan\left(\frac{\sqrt{x_{pos}^2+y_{pos}^2}}{z_{tower}}\right) \quad \text{(Equation 7)}$$

and θ_h is the azimuth angle of the heliostat relative to the tower base (anticlockwise from the South), *cf.* Equation 8:

$$\theta_h = \begin{cases} \theta_h = -90 - \arctan\left(\frac{y_{pos}}{|x_{pos}|}\right) & \text{if } x_{pos} \le 0 \\ \theta_h = 90 - \arctan\left(\frac{y_{pos}}{|x_{pos}|}\right) & \text{if } x_{pos} > 0 \end{cases} \quad \text{(Equation 8)}$$

The total direct irradiance impinging the receiver $P_{rec,tot}$ is calculated as the sum of the power effectively reflected by each heliostat, and is given by Equation 9:

$$P_{rec,tot} = \sum_{n=1}^{N_{hel}} P_{hel}\cdot\eta_{blocking}\cdot\sigma_{hel} = \sum_{n=1}^{N_{hel}} S_{hel}\cdot DNI\cdot\cos(\theta_{i,hel})\cdot\eta_{shadowing}\cdot\eta_{blocking}\cdot\sigma_{hel} \quad \text{(Equation 9)}$$

For the ST and the PVT model, the reflectivity of the heliostat σ_{hel} is assumed to be 0.9. For the PVM model, it is assumed to be 0.348 (total reflectance value calculated from the results of[60]).

Thermal balance of tower receivers (used by ST, PVT and PVM models)

If the total power absorbed by the receiver is greater than the expected thermal losses at nominal temperature (see Equation 11), then the output thermal power available is given by Equation 10,

$$P_{th} = P_{rec,tot} \cdot \eta_{loss} = P_{rec,tot} \cdot \left(\alpha - \frac{P_{loss,T_{nom}}}{P_{rec,tot}} \right) \quad \text{(Equation 10)}$$

where $P_{loss,T_{nom}}$ refers to the radiative (the receiver is assumed to be a grey body with a total emissivity of 0.9) and convective heat losses (with a constant and homogeneous convection heat transfer coefficient of 10 $W.m^{-2}.K^{-1}$) at the nominal operating temperature, and is given by:

$$P_{loss,T_{nom}} = P_{conv,T_{nom}} + P_{rad,T_{nom}} = S_{rec} \cdot \left[h_{conv} \cdot (T_{nom} - T_{amb}) + \varepsilon \cdot \sigma \cdot \left(T_{nom}^4 - T_{amb}^4 \right) \right] \quad \text{(Equation 11)}$$

The nominal operating temperatures considered for the estimation of the receiver's heat losses are summarized in the second table of this section.

Parabolic trough model (used by the PT model)

Parabolic trough (PT) technology is currently the most deployed CSP technology worldwide. Owing to the large amount of experimental data available in the literature, we select a semi-empirical PT model, which allows a simple, realistic and accurate description of the PT plants evaluated in this work. PT collectors usually follow a North-South orientation, and use synthetic oils typically operated between 290°C and 390°C as HTF. The total power absorbed at the receiver level is given by Equation 12,

$$P_{rec,tot,PT} = S_{PT} \cdot DNI \cdot \eta_{opt,PT} \cdot \eta_{shading,PT} \quad \text{(Equation 12)}$$

with:

- $\eta_{opt,PT}$, the optical efficiency of the PT, detailed in Equation 13, and retrieved from the experimental characterization of industrial PT rows given by Valenzuela et al.[61] These authors provided a semi-empirical equation correlating the system's optical efficiency to the angle of incidence of the solar rays on the aperture plane of the PT θ_i. This incidence angle θ_i is given by Equation 14.
- $\eta_{shading,PT}$ quantifies the *inter-row* shading (*i.e.* the shading caused by a row of troughs on the neighboring row) and is given by Equation 15.[62,63] $L_{spacing}$ refers to the distance separating two neighboring rows, and is taken equal to 18 m here. The "+" sign indicates that only positive values of the terms into brackets are taken into account, negative values leading to physically impossible negative shading efficiencies. Finally, $\theta_{tracking}$ is the PT collector tracking angle, given by Equation 16.[64]

$$\eta_{opt,PT} = 0.768 \cdot \left(\cos(\theta_{i,PT}) - 7 \cdot 10^{-4} \cdot \theta_{i,PT} - 36 \cdot 10^{-6} \cdot \theta_{i,PT}^2 \right) \quad \text{(Equation 13)}$$

$$\theta_{i,PT} = \arccos\left(\sqrt{1 - \cos(Az)^2 \cdot \cos(El)^2} \right) \quad \text{(Equation 14)}$$

$$\eta_{shading,PT} = 1 - \left[1 - \frac{L_{spacing}}{S_{PT}} \cdot \cos\left(\theta_{tracking}\right) \right]^+ \quad \text{(Equation 15)}$$

$$\theta_{tracking} = \arctan\left(\frac{\sin(Az)}{\tan(El)} \right) \quad \text{(Equation 16)}$$

If the total optical power $P_{rec,tot,PT}$ impinging the receiver exceeds the thermal losses at the receiver level $P_{loss,390°C}$, then the thermal power available at the receiver output $P_{th,PT}$ is given by Equation 17,

$$P_{th,PT} = P_{rec,tot,PT} - P_{loss,PT,l} \cdot L_{tot,PT} \quad \text{(Equation 17)}$$

with $P_{loss,PT,l}$ the thermal losses of the PT collectors, estimated through empirical correlations as a function of the average temperature difference inside the collectors $T_{mean,PT} = \frac{T_{390°C} + T_{290°C}}{2}$.[61]

$$P_{loss,PT,l} = 0.342 \cdot (T_{mean,PT} - T_{amb}) + 1.163 \cdot 10^{-8} \cdot (T_{mean,PT} - T_{amb})^4 \quad \text{(Equation 18)}$$

CSP power block model (ST, PVT, PVM and PT models)

The characteristics of the turbine and the inverter are tailored to match the electrical demand profile. Here, we assume that the peak nominal power of these two components corresponds to 95 % the maximal load power P_{TL} imposed to the solar plant over a year of operation.

For each CSP technology (PVM, PVT, ST, PT), the output power is written as the product between the total thermal power available and the efficiency of the power block, provided that the thermal power available at the receiver level exceeds the threshold power value above which the turbine starts. The electrical power delivered by the power block can simply be written:

$$P_{el} = \eta_{PB} \cdot P_{th} \quad \text{(Equation 19)}$$

with η_{PB} the power block efficiency, which is estimated from the nominal temperature T_{nom} (summarized for each technology in the table below), the Carnot efficiency η_{Carnot} and the exergy efficiency η_{ex} that takes into account the non-ideality of the power block, which has been taken equal to 0.66 in this work:[65]

$$\eta_{PB} = \eta_{ex} \cdot \eta_{Carnot} = \eta_{ex} \cdot \left(1 - \frac{T_{amb}}{T_{nom}}\right) \quad \text{(Equation 20)}$$

Technology	ST	PVT	PVM	PT
Temperature (°C)	560	400	560	390
η_{ex}	0.66	0.66	0.66	0.66

Photovoltaic module model (PVT, PVM, PV-TES and PV-TPVB models)

The solar radiation impinging the PV panels is a function of the solar technology considered: in the case of PVT systems, the input energy is equal to the total power gathered by the heliostats and reflected back to the receiver, and is given by Equation 9 (see section).

The PV-BESS, PV-TES and PV-TPVB models consider regular single-junction silicon PV cells which absorb and convert the global irradiation. The PV modules are assumed to be fixed, oriented toward the South in the Northern Hemisphere and toward the North in the Southern Hemisphere. Their inclination $\beta_{PV,SI}$ is equal to the latitude of the site, rounded to the nearest half decade (*i.e.* 40° at Targasonne, 35° at Phoenix and 20° at Antofagasta). Quito being located on the equator, the optimal inclination angle in this location should be 0°. However, because of the dust accumulation associated with the flat positioning of the PV panels in these circumstances, it was shown that small inclination angles would be preferable over flat positioning, and an inclination angle of 10° was thus chosen at this location.[66]

In the PVM model, the PV modules are used to reflect a fraction of the incoming sunlight to the receiver, located at the top of the tower. The solar resource available is thus dependent upon the heliostat orientation, the DNI and the DHI resource at each timestep.

Overall, the solar resource impinging the PV modules in the PVM, PV+BESS, PV+TES and PV+TPVB models is given by Equation 21,

$$P_{PV,in} = S_{PV} \cdot \left[DNI \cdot \cos(\theta_{i,mod}) \cdot \eta_{shadowing,mod} + DHI \cdot (1 + \cos(\beta_{mod})/2)\right] \quad \text{(Equation 21)}$$

with:

- $\theta_{i,mod}$ the incidence angle of the sunbeams onto the module. The incidence angle in the case of the PVM model, involving PV modules mounted onto tracking heliostats, is defined in Equation 6.
- $\eta_{shadowing,mod}$ the shadowing efficiency, which quantifies the area of the PV modules effectively exposed to sunlight. The shadowing in the PVM model in calculated at each timestep and for each heliostat using SolarPilot. In the PV+BESS, PV+TES and PV+TPVB models, it is calculated at each time step based on the equations provided in.[67–70]
- β_{mod} the inclination angle of the module, which is detailed above for conventional PV modules, and which is given in Equation 22 [71] for the PVT approach involving heliostat tracking.

$$\beta_{hel} = \arcsin\left(\frac{\cos(\lambda) + \sin(El)}{2 \cdot \cos(\theta_{i,hel})}\right) \quad \text{(Equation 22)}$$

The PV power output is given by Equation 23,

$$P_{PV} = F_{PV} \cdot \eta_{PV,theo} \cdot k_{Temp} \cdot \eta_{inverter} \cdot P_{PV,in} \quad \text{(Equation 23)}$$

with $\eta_{inverter}$ the inverter efficiency, $\eta_{PV,theo}$ the theoretical maximum efficiency of the PV cell (depending on technology), F_{PV} the PV cell's ability to approach its own theoretical limit, and k_{Temp} a temperature coefficient of the PV cell that drives the power loss due to the temperature increase, given by Equation 24.

$$k_{Temp} = (1 + \beta_{ref} \cdot (T_{PV} - T_{STC,ref})) \quad \text{(Equation 24)}$$

The different values that were taken for each technology are summarized in the following table.

Model	F_{PV}	$\eta_{inverter}$	β_{ref} $[K^{-1}]$	$\eta_{PV,theo}$
PVT	0.65	0.978	X	η_{PVT}
PVM	0.76	0.978	-0.0008	0.33
PV	0.62	0.978	-0.0037	0.32

Several asumptions were formulated regarding the operation of the different PV converters:

- F_{PV} is a particularly difficult indicator to estimate for technologies that still require significant research and development efforts prior to their practical implementation: In the case of PVT technology, a value of 0.65 has been arbitrarily set. To date, the first experimental characterizations of PV cells operating at 400°C have demonstrated a F_{PV} value close to 0.35.[43,44,72] The estimates provided in this work therefore assume a significant improvement in the ability of PVT cells to approach their own theoretical limits. In the case of PVM technology, which is based on the use of photovoltaic mirrors based on GaAs technology, a value of FPV equal to 0.76 has been set. This value is identical to those of the best GaAs modules reported in the literature to date[73] In the case of Silicon PV modules using PV+TES, PV+BESS and PV+TPVB technologies, a FPV value equal to 0.62 has been chosen. This value is equivalent to that of Silicon technologies commonly deployed in industrial PV plants %($\eta \sim 20$).
- The theoretical efficiency of Si and GaAs cell technologies are determined based on the detailed balance formalism.[74] In the specific case of "high temperature" cells used in the PVT approach, the conversion efficiency is calculated at each time step taking into account the solar concentration factor at the PVT receiver.
- The temperature coefficients of GaAs and Si technologies are taken from[75] and[76] In the case of the PVT approach, a constant receiver temperature equal to 400°C is assumed.

$T_{STC,ref}$ is the standard condition test temperature (25°C) and T_{PV} the theoretical equilibrium temperature of the illuminated PV cell, which is detailed in Equation 25,[77]

$$T_{PV} = T_{amb} + (T_{NOCT} - T_{amb}) \cdot \frac{GHI}{G_{NOCT}} \cdot \frac{U_{NOCT}}{U_L} \quad \text{(Equation 25)}$$

with:

- $T_{NOCT} = 46°C$ the normal operating temperature of the cell exposed to $G_{NOCT} = 800\ W.m^{-2}$, and with heat losses characterized by an overall coefficient $U_{NOCT} = 9.53\ W.m^{-2}.K^{-1}$;
- $T_{amb} = 20°C$ the ambient temperature in the standard test conditions;
- $U_L = 5.67 + 3.86 \cdot U_{wind}$ the heat transfer coefficient between the cell and the environment, which depends on the wind speed U_{wind}, itself given by the weather file.

Annual energy production

The annual energy delivered by each plant are obtained by summing the hourly energy productions, considering a time step Δt of 1 h between two consecutive calculations (see Equation 26).

$$E_{an,plant} = \sum_{h=1}^{h=8760} P_{el,plant}(h) \cdot \Delta t \quad \text{(Equation 26)}$$

Energy storage model

Energy storage systems are modelled as perfect charging and discharging batteries. The size of the storage systems is given by Equation 27, with $\Delta_{t,storage}$ the duration of the storage system, which is a variable in the parametric study, $P_{average,plant}$ the average power that is produced by the plant along the year, given in Equation 28, $SOC_{max,ES}$ and $SOC_{in,ES}$ the maximum and minimum state of charge (SOC) of the energy storage (ES) systems.

$$E_{ES,capacity} = \frac{P_{average,plant} \cdot \Delta_{t,storage}}{\eta_{rt,ES} \cdot (SOC_{max,ES} - SOC_{min,ES})} \quad \text{(Equation 27)}$$

The values of these variables are listed in the table below.

Energy storage technology	SOC_{min} - SOC_{max}	$\eta_{rt,ES}$	$\eta_{self-discharge}$
TES @ ~ 560°C	0.02 - 0.98	$\eta_{PB,T_{nom}}$	99.95 %[78]
TES @ ~ 400°C	0.02 - 0.98	$\eta_{PB,T_{nom}}$	99.97 %[78]
BESS	0.10 - 0.90[79]	0.925[79]	99.99 %[78,80]
TPVB	0.02 - 0.98	0.4[42]	99.8 %[41]

Demand

The demand profile applied to each plant investigated is derived as follows:

1. the maximum electrical energy a specific technology can inject into the grid over a year, is calculated with Equation 26 (assuming that the electrical energy produced is directly injected into the grid);
2. the *mean power production*, corresponding to the power that should be continuously generated by the plant over a year to deliver the same energy is calculated with Equation 28

$$P_{average,plant} = E_{an,plant}/N_{hours,year} = E_{an,plant}/8760 \quad \text{(Equation 28)}$$

3. a normalized demand curve is derived considering the actual country demand $P_{demand,country}$:

$$P_{demand,norm}(t) = \frac{P_{demand,country}(t)\cdot 1}{\sum_{h=1}^{h=8760} P_{demand,country}\cdot \Delta t} \quad \text{(Equation 29)}$$

4. the instantaneous demand for a specific power plant $P_{demand,plant}$ is obtained by multiplying the normalized demand, the average power production of the plant, and a demand factor f quantifying the degree of solicitation of the plant relative to the average power $P_{average,plant}$. If $f = 1$, then the total energy demanded from the plant is equal to the maximum electrical energy $E_{an,plant}$. If $f < 1$, then the energy demanded from the plant is lower than this reference value, promoting energy storage. Conversely, f values exceeding 1 promote a direct injection of the electricity generated by the plant on the electrical grid, and lower the amount of energy available for storage and delayed use. The instantaneous power demanded from the plant can be written:

$$P_{demand,plant}(t) = P_{demand,norm}\cdot f\cdot P_{average,plant} \quad \text{(Equation 30)}$$

Power block sizing and minimum working values

The nominal power of the power block, if relevant, is set as 95 % of the maximum power that can be demanded from the grid, *cf.* Equation 31. The minimum power below which the power block is not operating is set as 30 % of the latter, *cf.* Equation 32.

$$P_{PB,nom} = 0.95\cdot max\left(P_{demand,country}\right)\cdot f \quad \text{(Equation 31)}$$

$$P_{PB,min} = 0.3\cdot P_{PB,nom} \quad \text{(Equation 32)}$$

For PV and TPV systems, no minimum threshold power values are considered.

Parametric study

For the 7 different power plants, the main performance indicators are investigated as a function of two operating parameters:

- the energy storage duration $\Delta_{t,storage}$, which ranges from 0 h to 30 h;
- the load fraction f, which ranges from 0 to 2.

Energy storage management

The injection of electrical energy on the grid and the storage of the surplus energy follows the strategy described below:

1. Charge:

- The electrical power generated by the plant is calculated for each time step, provided that the power block's inlet available energy is higher than the threshold power value below which the turbine cannot be operated;
- If the electrical power generated exceeds the demand, the latter is satisfied and the surplus energy is sent to the storage system, provided that the SOC is sufficiently low. If the surplus energy is higher than the remaining storage capacity, then the difference is curtailed;
- In the case of hybrid systems (PVM and PVT), the electrical demand is primarily met by PV electricity. The CSP energy is then either used to complement the missing fraction of the electricity demand non-delivered by the PV subsystem, or stored as heat. If the PV production exceeds the electrical demand, then the remaining PV electricity is stored as heat using resistive heating;
- If the sum of the plant's production and the energy available in the storage is not sufficient to satisfy $P_{PB,min}$ (minimum power required to start the power block), then the energy generated is entirely stored.

2. Discharge:
   - If the electrical power generated by the plant is lower than the demand but higher than $P_{PB,min}$, then it is fully injected into the grid, and the missing energy is taken from the energy storage system, provided that its state of charge is high enough;
   - If the energy remaining in the storage is not sufficient to satisfy the remaining demand, the storage is discharged to its $SOC_{min,ES}$ value and the remaining fraction of the energy demand is not satisfied.

Economic model

CAPEX, OPEX and LCOE

The different costs were divided into capital expenditures (CAPEX) and operational expenditures (OPEX), each of them being also subdivided into different cost contributions associated with the main components of the power plants, differentiating cost per power and cost per energy capacity. The assumptions used for the different CAPEX calculations are summarized in Tables S1 and S2. The costs are expressed in euros considering an exchange rate of 1.2 US dollar/euro. The cost estimates for 2030 are given in 2020 euros.

ST plants. The CAPEX of a Solar Tower plant is a function of its direct costs DC_{ST}, *i.e.* the costs of the heliostat field $DC_{hel,ST}$, the tower $DC_{T,ST}$, the receiver $DC_{rec,ST}$, the power block $DC_{PB,ST}$, the thermal energy storage system $DC_{TES,ST}$ and the balance of plant $DC_{BoP,ST}$, plus all the proportional costs associated with EPC (engineering, procurement and construction), labour and others, respectively estimated with proportional factors $k_{epc,ST}$, $k_{lab,ST}$ and $k_{oth,ST}$ that are applied to the other direct costs. A contingency cost, proportional to the former total cost, has also to be applied.

$$CAPEX_{ST} = \left(DC_{ST} \cdot \left\{1 + \left[k_{epc} + k_{lab} + k_{oth}\right]_{ST}\right\} + IC_{ST}\right) \cdot (1 + k_{c,ST}) \quad \text{(Equation 33)}$$

$$DC_{ST} = \left[DC_{hel} + DC_{T} + DC_{rec} + DC_{TES} + DC_{PB} + DC_{BoP}\right]_{ST} \quad \text{(Equation 34)}$$

$$DC_{hel,ST} = C_{hel,ST} \cdot N_{hel,ST} \cdot S_{hel,ST} \quad \text{(Equation 35)}$$

$$DC_{t,ST} = C_{t,ST} \cdot H_{tower} \quad \text{(Equation 36)}$$

$$DC_{rec,ST} = C_{rec,ST} \cdot P_{rec,ST} \quad \text{(Equation 37)}$$

$$DC_{TES,ST} = C_{TES,ST} \cdot E_{TES,ST} \quad \text{(Equation 38)}$$

$$DC_{PB,ST} = C_{PB,ST} \cdot P_{nom,ST} \quad \text{(Equation 39)}$$

$$DC_{BoP,ST} = C_{BoP,ST} \cdot P_{nom,ST} \quad \text{(Equation 40)}$$

The indirect cost of solar towers are only associated with site improvement:

$$IC_{ST} = IC_{land,ST} = C_{land,ST} \cdot 6.459 \cdot N_{hel,ST} \cdot S_{hel,ST} \quad \text{(Equation 41)}$$

PV-BESS plants. The capital expenditure $CAPEX_{PVBES}$ depends on the cost of PV modules, $DC_{mod,PV}$, the cost of batteries, DC_{bat}, inverter, $DC_{inv,PV}$, structural components of PV and BESS, respectively $DC_{str,PV}$ and $DC_{str,BES}$ and the electrical components $DC_{el,PV}$ and $DC_{el,BES}$.

$$CAPEX_{PVBES} = \left(DC_{PVBES} \cdot \left\{1 + \left[k_{epc} + k_{lab} + k_{oth}\right]_{PV}\right\} + IC_{PV}\right) \cdot (1 + k_{c,PV}) \quad \text{(Equation 42)}$$

$$DC_{PVBES} = [DC_{mod} + DC_{inv} + DC_{el} + DC_{str}]_{PV} + [DC_{bat} + DC_{str} + DC_{el}]_{BES} \quad \text{(Equation 43)}$$

$$DC_{mod,PV} = C_{mod,PV} \cdot N_{modPV} \cdot S_{modPV} \cdot GHI_{ref} \cdot \varepsilon_{modPV,nom} / 1000 \quad \text{(Equation 44)}$$

$$DC_{bat,BES} = E_{BES} \cdot (C_{bat} + C_{bat,8} + C_{bat,16}) \quad \text{(Equation 45)}$$

$$DC_{inv,PV} = C_{inv,PV} \cdot P_{nom,PV} \quad \text{(Equation 46)}$$

$$DC_{str,PV} = C_{str,PV} \cdot N_{mod,PV} \cdot S_{mod,PV} \cdot GHI_{ref} \cdot \varepsilon_{mod,PV,nom} \quad \text{(Equation 47)}$$

$$DC_{str,BES} = C_{str,BES} \cdot P_{nom,PV} \quad \text{(Equation 48)}$$

$$DC_{el,PV} = C_{el,PV} \cdot N_{mod,PV} \cdot S_{mod,PV} \cdot GHI_{ref} \cdot \varepsilon_{modPV,nom} \quad \text{(Equation 49)}$$

$$DC_{el,BES} = C_{el,BES} \cdot P_{nom,PV} \quad \text{(Equation 50)}$$

$$IC_{PVBES} = IC_{land,PVBES} = C_{land,PVBES} \cdot 6.459 \cdot N_{hel,ST} \cdot S_{hel,ST} \quad \text{(Equation 51)}$$

PVT plants. PVT plants share a large number of cost components with conventional ST plants, however the integrated PV/CSP receiver is necessarily more complex than its conventional CSP counterpart, leading to an extra cost of the former. Hybrid PV/CSP plants also share inverter cost components with conventional PV plants.

$$CAPEX_{PVT} = \left(DC_{PVT} \cdot \left\{1 + [k_{epc} + k_{lab} + k_{oth}]_{ST}\right\} + IC_{ST}\right) \cdot (1 + k_{c,ST}) \quad \text{(Equation 52)}$$

$$DC_{PVT} = [DC_{hel} + DC_t]_{ST} + [DC_{rec} + DC_{TES} + DC_{PB} + DC_{BoP} + DC_{inv} + DC_{land}] \quad \text{(Equation 53)}$$

$$DC_{rec,PVT} = C_{rec,PVT} \cdot P_{rec,PVT} = C_{rec,PVT} \cdot P_{rec,ST} \quad \text{(Equation 54)}$$

$$DC_{TES,PVT} = C_{TES,ST} \cdot E_{TES,PVT} \quad \text{(Equation 55)}$$

$$DC_{PB,PVT} = C_{PB,ST} \cdot P_{nom,PVT} \quad \text{(Equation 56)}$$

$$DC_{BoP,PVT} = C_{BoP,ST} \cdot P_{nom,PVT} \quad \text{(Equation 57)}$$

$$DC_{inv,PVT} = C_{inv,PV} \cdot P_{nom,PVT} \quad \text{(Equation 58)}$$

PVM plants. The CAPEX of PVM plants is estimated taking into account the hybrid nature of the heliostats (acting both as reflectors and PV converters) and thus, their extra-cost in comparison with conventional mirror-based heliostats.

$$CAPEX_{PVM} = \left(DC_{PVM} \cdot \left\{1 + [k_{epc} + k_{lab} + k_{oth}]_{ST}\right\} + IC_{ST}\right) \cdot (1 + k_{c,ST}) \quad \text{(Equation 59)}$$

$$DC_{PVM} = DC_{t,ST} + [DC_{hel} + DC_{rec} + DC_{TES} + DC_{PB} + DC_{BoP} + DC_{inv}]_{PVM} \quad \text{(Equation 60)}$$

$$DC_{hel,PVM} = C_{hel,PVM} \cdot N_{hel,ST} \cdot S_{hel,ST} \quad \text{(Equation 61)}$$

$$DC_{rec,PVM} = C_{rec,ST} \cdot DNI_{ref} \cdot N_{hel,ST} \cdot S_{hel,ST} \cdot \varepsilon_{mod,PVM,th} \quad \text{(Equation 62)}$$

$$DC_{TES,PVM} = C_{TES,ST} \cdot E_{TES,PVM} \quad \text{(Equation 63)}$$

$$DC_{PB,PVM} = C_{PB,ST} \cdot P_{nom,PVM} \quad \text{(Equation 64)}$$

$$DC_{BoP,PVM} = C_{BoP,ST} \cdot P_{nom,PVM} \quad \text{(Equation 65)}$$

$$DC_{inv,PVM} = C_{inv,PV} \cdot P_{nom,PVM} \quad \text{(Equation 66)}$$

PV-TES plants. The cost components of PV-TES plants are very similar to those of conventional PV plants, and include additional cost components associated with the presence of TES system (i.e. heat storage and turbine).

$$CAPEX_{PVTES} = \left(DC_{PVTES} \cdot \left\{1 + \left[k_{epc} + k_{lab} + k_{oth}\right]_{PV}\right\} + IC_{PV}\right) \cdot (1 + k_{c,PV}) \quad \text{(Equation 67)}$$

$$DC_{PVTES} = \left[DC_{mod} + DC_{inv} + DC_{comp} + DC_{elec}\right]_{PV} + DC_{TES} + DC_{PB,PVTES} \quad \text{(Equation 68)}$$

$$DC_{TES,PV} = C_{TES,ST} \cdot E_{TES,PVTES} \quad \text{(Equation 69)}$$

$$DC_{PB,PVTES} = C_{PB,ST} \cdot P_{nom,PV} \quad \text{(Equation 70)}$$

$$DC_{land,PVBES} = C_{land,PVBES} \cdot 6.459 \cdot N_{hel,ST} \cdot S_{hel,ST} \quad \text{(Equation 71)}$$

PV-TPV plants. The costs components of PV+TPVB plants are similar to those of PV+TES, but include the costs components of this particular storage technology instead of those of TES. In addition, the contingency costs are taken equal to those of ST, because of the financial risks associated with the development of this new technology.

$$CAPEX_{PVTPV} = \left(DC_{PVTPV} \cdot \left\{1 + \left[k_{epc} + k_{lab} + k_{oth}\right]_{PV}\right\} + IC_{PV}\right) \cdot (1 + k_{c,ST}) \quad \text{(Equation 72)}$$

$$DC_{PVTPV} = \left[DC_{mod} + DC_{inv} + DC_{str} + DC_{el}\right]_{PV} + DC_{TPV} \quad \text{(Equation 73)}$$

$$DC_{TPV} = C_{TPV,E} \cdot E_{PVTPV} \cdot \varepsilon_{TPV} + C_{TPV,P} \cdot P_{nom,PV} \quad \text{(Equation 74)}$$

$$DC_{str,TPV} = C_{str,BES} \cdot P_{nom,PV} \quad \text{(Equation 75)}$$

$$DC_{el,TPV} = C_{el,BES} \cdot P_{nom,PV} \quad \text{(Equation 76)}$$

$$IC_{land,TPV} = C_{land,ST} \cdot 4.9318 \cdot N_{hel,ST} \cdot S_{hel,ST} \quad \text{(Equation 77)}$$

PT plants. The cost components of PT plants are similar to those of ST power plants, but also include specific cost components.

$$CAPEX_{PT} = \left(DC_{PT} \cdot \left\{1 + \left[k_{epc} + k_{lab} + k_{oth}\right]_{PT}\right\} + IC_{PT}\right) \cdot (1 + k_{c,ST}) \quad \text{(Equation 78)}$$

$$DC_{PT} = DC_{PTC} + \left[DC_{HTF} + DC_{TES} + DC_{PB} + DC_{BoP}\right]_{PT} \quad \text{(Equation 79)}$$

$$DC_{PTC} = C_{PTC} \cdot N_{hel,ST} \cdot S_{hel,ST} \quad \text{(Equation 80)}$$

$$DC_{HTF,PT} = C_{HTF,PT} \cdot N_{hel,ST} \cdot S_{hel,ST} \quad \text{(Equation 81)}$$

$$DC_{TES,PT} = C_{TES,PT} \cdot E_{TES,PT} \quad \text{(Equation 82)}$$

$$DC_{PB,PT} = C_{PB,ST} \cdot P_{nom,PT} \quad \text{(Equation 83)}$$

$$DC_{BoP,PT} = C_{BoP,PT} \cdot P_{nom,PT} \quad \text{(Equation 84)}$$

$$IC_{PT} = IC_{land,PT} = C_{land,PT} \cdot 5.2484 \cdot N_{hel,ST} \cdot S_{hel,ST} \quad \text{(Equation 85)}$$

The operation and maintenance costs are subdivided into three components:

$$OPEX_{plant} = OPEX_{plant,power} + OPEX_{plant,energy} + k_i \cdot CAPEX \quad \text{(Equation 86)}$$

With k_i the insurance rate, taken equl to 1 %;[79] the insurance cost is directly proportional to the CAPEX.

From those values, the levelized costs of electricity (LCOE) is calculated with Equation 87.

$$LCOE = \frac{(k_a + k_i) \cdot CAPEX + OPEX_{an}}{\tau_{\mathrm{deg},plant} \cdot E_{an,plant}} \quad \text{(Equation 87)}$$

with $\tau_{\mathrm{deg},plant}$ representing the levelized degradation of the plant over its entire lifetime (91.4% for PV plants[36] and 93.75% for CSP plants[63]), and k_a a capital recovery factor, given in Equation 88.

$$k_a = \frac{r \cdot (1+r)^{N_{years}}}{(1+r)^{N_{years}} - 1} \quad \text{(Equation 88)}$$

All the costs data used for the 2020 and 2030 cost evaluation, along with their references, are provided in Tables S1 and S2. In the absence of any commercial deployment of PVT and PVM hybrid technologies, the prices of the PV mirrors in the PVM approach, and of the PVT receiver (PVT approach) were arbitrarily set to 1.5 time the price of conventional heliostat (a value deduced from the replacement of the mirrors ($\sim$ 20 % of the heliostat cost) by Si PV modules), and to 1.3 times the price of conventional receiver (a value deduced from the integration of $III-V$ solar cells onto the surface of the thermal receiver).